VON KARMAN INSTITUTE FOR FLUID DYNAMICS
CHAUSSÉE DE WATERLOO, 72
B - 1640 RHODE SAINT GENÈSE, BELGIUM

PROJECT REPORT 1984-14 JUNE 1984

EXPLICIT RUNGE-KUTTA ARTIFICIAL COMPRESSIBILITY TECHNIQUE FOR INCOMPRESSIBLE NAVIER-STOKES EQUATIONS

APPLICATION TO THE BACKWARD FACING STEP FLOW

BARRY KOREN

SUPERVISOR : J.-A. ESSERS

ACKNOWLEDGEMENTS

I am grateful to Professor Essers for his introductory lessons given from October 1983 to January 1984, which after having obtained the first good results (beginning month June) appeared to have been very valid and solid.
I am grateful to Mart Borsboom for his useful advises during the whole month June, and especially for his offer to use his excellent plot-program.

ABSTRACT

Given in this report is a solution technique for the 2-dimensional, incompressible Navier-Stokes equations for Reynolds numbers much larger than 1.
Given also in this report are results obtained with this solution technique, for the steady backward facing step flow. Results have been obtained for a Reynolds number of 50. No results have been obtained for Reynolds numbers higher than 50.

CONTENTS page

NOTATIONS

symbols

b	constant in front of the space derivatives of the unsteady continuity equation
ccx	weight coefficient for the contribution of the pressure gradient in x-direction at the concave corner of the step, to the weighted pressure gradient at that corner
ccy	weight coefficient for the contribution of the pressure gradient in y-direction at the concave corner of the step, to the weighted pressure gradient at that corner
cvx	weight coefficient for the contribution of the pressure gradient in x-direction at the convex corner of the step, to the weighted pressure gradient at that corner
cvy	weight coefficient for the contribution of the pressure gradient in y-direction at the convex corner of the step, to the weighted pressure gradient at that corner
j	index used for horizontal mesh lines
k	wave number
m	index used for vertical mesh lines
nx_{inlet}	number of vertical mesh lines from the inlet up to and including the vertical wall of the step
nx_{outlet}	number of vertical mesh lines from the vertical wall of the step up to and including the outlet
ny_{inlet}	number of horizontal mesh lines from the lower wall of the inlet part up to and including the upper wall
ny_{step}	number of horizontal mesh lines from the lower wall of the outlet part up to and including the lower wall of the inlet part
p	pressure
Re	Reynolds number based on the maximum velocity component in x-direction at the inlet, and on the step height in the physical domain
t	time
u	velocity component in x-direction
v	velocity component in y-direction
x	coordinate in the physical domain
$\bar{x}$	coordinate in the computational domain
y	coordinate in the physical domain
$\bar{y}$	coordinate in the computational domain
λ	eigenvalue
μ	dynamic viscosity
ρ	density
ω	$\sqrt{\omega_x^2+\omega_y^2}$

ω_x	frequency x-dependent Fourier-component
ω_y	frequency y-dependent Fourier-component

subscripts

step	convex corner of the step
upper	upper wall

1. INTRODUCTION

The 2-dimensional, incompressible Navier-Stokes equations, describing a steady flow problem are

$$\left.\begin{aligned} &\frac{\partial u}{\partial x}+\frac{\partial v}{\partial y}=0 \\ &\rho\left(u\frac{\partial u}{\partial x}+v\frac{\partial u}{\partial y}\right)=-\frac{\partial p}{\partial x}+\mu\left(\frac{\partial^2 u}{\partial x^2}+\frac{\partial^2 u}{\partial y^2}\right) \\ &\rho\left(u\frac{\partial v}{\partial x}+v\frac{\partial v}{\partial y}\right)=-\frac{\partial p}{\partial y}+\mu\left(\frac{\partial^2 v}{\partial x^2}+\frac{\partial^2 v}{\partial y^2}\right) \end{aligned}\right\} \quad (1.1)$$

Introducing the non-dimensional quantities

$$\left.\begin{aligned} u&=\frac{u}{u_{ref}} \\ v&=\frac{v}{u_{ref}} \\ p&=\frac{p}{p_{ref}} \\ x&=\frac{x}{L_{ref}} \\ y&=\frac{y}{L_{ref}} \end{aligned}\right\} \quad (1.2)$$

system (1.1) can be rewritten in the following form

$$\left.\begin{aligned} &\frac{\partial u}{\partial x}+\frac{\partial v}{\partial y}=0 \\ &u\frac{\partial u}{\partial x}+v\frac{\partial u}{\partial y}=-\frac{\partial p}{\partial x}+\frac{\mu}{\rho_{ref}u_{ref}L_{ref}}\left(\frac{\partial^2 u}{\partial x^2}+\frac{\partial^2 u}{\partial y^2}\right) \\ &u\frac{\partial v}{\partial x}+v\frac{\partial v}{\partial y}=-\frac{\partial p}{\partial y}+\frac{\mu}{\rho_{ref}u_{ref}L_{ref}}\left(\frac{\partial^2 v}{\partial x^2}+\frac{\partial^2 v}{\partial y^2}\right) \end{aligned}\right\} \quad (1.3)$$

Introducing next

$$Re=\frac{\rho_{ref}\,u_{ref}\,L_{ref}}{\mu} \quad (1.4)$$

the 2-dimensional, incompressible Navier-Stokes equations become in non-dimensional form

$$\left.\begin{aligned} &\frac{\partial u}{\partial x}+\frac{\partial v}{\partial y}=0 \\ &u\frac{\partial u}{\partial x}+v\frac{\partial u}{\partial y}=-\frac{\partial p}{\partial x}+\frac{1}{Re}\left(\frac{\partial^2 u}{\partial x^2}+\frac{\partial^2 u}{\partial y^2}\right) \\ &u\frac{\partial v}{\partial x}+v\frac{\partial v}{\partial y}=-\frac{\partial p}{\partial y}+\frac{1}{Re}\left(\frac{\partial^2 v}{\partial x^2}+\frac{\partial^2 v}{\partial y^2}\right) \end{aligned}\right\} \quad (1.5)$$

A well-known iterative technique to solve this system of equations is to solve at first the Poisson equation for the pressure

$$\Delta p^{\ell+1}=\frac{1}{Re}\Delta\left(\frac{\partial u}{\partial x}+\frac{\partial v}{\partial y}\right)^{\ell}-\frac{\partial}{\partial x}\left(u\frac{\partial u}{\partial x}+v\frac{\partial u}{\partial y}\right)^{\ell}-\frac{\partial}{\partial y}\left(u\frac{\partial v}{\partial x}+v\frac{\partial v}{\partial y}\right)^{\ell} \quad (1.6)$$

, which can be obtained form both momentum equations, and in which the supersript ℓ and $\ell+1$ indicate two successive iteration levels. Using the continuity equation above Poisson equation simplifies to

$$\Delta p^{\ell+1}=-\frac{\partial}{\partial x}\left(u\frac{\partial u}{\partial x}+v\frac{\partial u}{\partial y}\right)^{\ell}-\frac{\partial}{\partial y}\left(u\frac{\partial v}{\partial x}+v\frac{\partial v}{\partial y}\right)^{\ell} \quad (1.7)$$

Using the known pressure at iteration level $\ell+1$ the following Poisson equation for respectively u and v at iteration level $\ell+1$ can be solved

$$\Delta u^{\ell+1}=\frac{1}{Re}\left\{\frac{\partial p}{\partial x}^{\ell+1}+\left(u\frac{\partial u}{\partial x}+v\frac{\partial u}{\partial y}\right)^{\ell}\right\} \quad (1.8)$$

$$\Delta v^{\ell+1}=\frac{1}{Re}\left\{\frac{\partial p}{\partial y}^{\ell+1}+\left(u\frac{\partial v}{\partial x}+v\frac{\partial v}{\partial y}\right)^{\ell}\right\} \quad (1.9)$$

A simpler solution technique which avoids the cumbersome solution of a Poisson equation for both u,v and p at each iteration level has been chosen. Chosen has been the solution technique introduced by Chorin (ref.1). In the solution technique introduced by Chorin the 2-dimensional, incompressible Navier-Stokes equations are solved by marching in time, using the system of equations

$$\left.\begin{aligned} &\frac{\partial p}{\partial t}+b\left(\frac{\partial u}{\partial x}+\frac{\partial v}{\partial y}\right)=0 \\ &\frac{\partial u}{\partial t}+u\frac{\partial u}{\partial x}+v\frac{\partial u}{\partial y}=-\frac{\partial p}{\partial x}+\frac{1}{Re}\left(\frac{\partial^2 u}{\partial x^2}+\frac{\partial^2 u}{\partial y^2}\right) \\ &\frac{\partial v}{\partial t}+u\frac{\partial v}{\partial x}+v\frac{\partial v}{\partial y}=-\frac{\partial p}{\partial y}+\frac{1}{Re}\left(\frac{\partial^2 v}{\partial x^2}+\frac{\partial^2 v}{\partial y^2}\right) \end{aligned}\right\} \quad (1.10)$$

The solution of the original system (1.5) will have been obtained

as soon as in the time marching procedure the steady state has been reached; i.e. as soon as the time derivatives in (1.10) can be neglected with respect to the space derivatives.
The constant b has been introduced in the continuity equation as a constant to be used for the optimization of the rate of convergence of the time marching procedure.
Concerning the time discretization: chosen can be between an explicit or implicit time discretization. When Chorin introduced the artificially time-dependent system (1.10), no good explicit time discretizations were available; i.e. no time discretizations which were stable for flows for which $Re \geq 1$. Nowadays these time discretizations do exist. Nowadays the choice can therefore be made between an explicit or implicit time discretization. Chosen has been an explicit time discretization; chosen has been: Runge-Kutta.
Concerning the space discretization: chosen can be between a finite difference, a finite volume or a finite element discretization. Chosen has been a finite difference discretization; chosen has been the five-points scheme given in fig.1.1.

For the considered flow problem; the backward facing step flow, use could be made of various computational results presented at a GAMM Workshop (ref.2), and also of computational results recently obtained at VKI with an implicit time discretization and a finite volume space discretization.

2. COMPUTATIONAL METHOD

2.1. Stretching

In order to have a sufficient number of points in flow regions with large gradients, but also a total number of points which is as small as the accuracy allows, a non-equidistant mesh has been used. For simplicity the space discretization has not been performed in the non-equidistant mesh in the physical domain, but in an equidistant mesh in the computational domain. Both meshes are related with each other by stretching functions. Using as x,y-coordinate system in the physical domain, the coordinate system given in fig.2.1, and using the notations $\bar{x}$ and $\bar{y}$ for the coordinates in the computational domain, the stretching functions used can be written in the following way

$$x(\bar{x}) = \frac{x_1}{e^{power}-1}\left(e^{power\,\frac{\bar{x}_{step}-\bar{x}}{\bar{x}_{step}-\bar{x}_1}}-1\right) \tag{2.1}$$

with for

$$\left.\begin{aligned} x \leqslant 0: \quad & x_1 = \bar{x}_1 = x_{inlet} \\ x \geqslant 0: \quad & x_1 = \bar{x}_1 = x_{outlet} \end{aligned}\right\} \tag{2.2}$$

and

$$y(\bar{y}) = \frac{y_2-y_1}{e^{power}-1}\left(e^{power\,\frac{\bar{y}-\bar{y}_1}{\bar{y}_2-\bar{y}_1}}-1\right)+y_1 \tag{2.3}$$

with for

$$\left.\begin{aligned} 0 \leqslant y \leqslant \frac{y_{step}}{2}: \quad & y_1=0,\ y_2=\frac{y_{step}}{2},\ \bar{y}_1=0,\ \bar{y}_2=\frac{\bar{y}_{step}}{2} \\ \frac{y_{step}}{2} \leqslant y \leqslant y_{step}: \quad & y_1=y_{step},\ y_2=\frac{y_{step}}{2},\ \bar{y}_1=\bar{y}_{step},\ \bar{y}_2=\frac{\bar{y}_{step}}{2} \\ y_{step} \leqslant y \leqslant \frac{y_{step}+y_{upper}}{2}: \quad & y_1=y_{step},\ y_2=\frac{y_{step}+y_{upper}}{2},\ \bar{y}_1=\bar{y}_{step},\ \bar{y}_2=\frac{\bar{y}_{step}+\bar{y}_{upper}}{2} \\ \frac{y_{step}+y_{upper}}{2} \leqslant y \leqslant y_{upper}: \quad & y_1=y_{upper},\ y_2=\frac{y_{step}+y_{upper}}{2},\ \bar{y}_1=\bar{y}_{upper},\ \bar{y}_2=\frac{\bar{y}_{step}+\bar{y}_{upper}}{2} \end{aligned}\right\} \tag{2.4}$$

For $\bar{x}_{step}$, $\bar{y}_{step}$ and $\bar{y}_{upper}$ it holds

$$\left.\begin{aligned}
\bar{x}_{step} &= \frac{(nx_{inlet}-1)\,x_{outlet} + (nx_{outlet}-1)\,x_{inlet}}{(nx_{inlet}-1)+(nx_{outlet}-1)} \\
\bar{y}_{step} &= \frac{(ny_{step}-1)\,y_{upper}}{(ny_{step}-1)+(ny_{inlet}-1)} \\
\bar{y}_{upper} &= y_{upper}
\end{aligned}\right\} \quad (2.5)$$

in which is:

- nx_{inlet}: the number of vertical mesh lines from the inlet up to and including the vertical wall of the step,
- nx_{outlet}: the number of vertical mesh lines from the vertical wall of the step up to and including the outlet,
- ny_{step}: the number of horizontal mesh lines from the lower wall of the outlet part up to and including the lower wall of the inlet part, and
- ny_{inlet}: the number of horizontal mesh lines from the lower of the inlet part up to and including the upper wall.

With the constant power in respectively (2.1) and (2.3) the stretching can be changed; the larger the power, the more stretched the mesh.

2.2. Runge-Kutta schemes

In order to discuss the Runge-Kutta schemes, consider the system of equations

$$\frac{\partial \vec{s}}{\partial t} = F(\vec{s}) \quad (2.6)$$

with in the left hand side the time-dependent part and in the right hand side the space operator. Consider now to be known the solution $\vec{s}$ at iteration level ℓ, and to be computed the solution $\vec{s}$ at the next iteration level; iteration level $\ell+1$.
A general Runge-Kutta scheme, i.e. a Runge-Kutta scheme consisting of n steps has the following form

$$\left.\begin{aligned}
\vec{s}^{\,1} &= \vec{s}^{\,\ell} + a_1 \Delta t\, F(\vec{s}^{\,\ell}) \\
\vec{s}^{\,2} &= \vec{s}^{\,\ell} + a_2 \Delta t\, F(\vec{s}^{\,1}) + b_2 \Delta t\, F(\vec{s}^{\,\ell}) \\
\vec{s}^{\,3} &= \vec{s}^{\,\ell} + a_3 \Delta t\, F(\vec{s}^{\,2}) + b_3 \Delta t\, F(\vec{s}^{\,1}) + c_3 \Delta t\, F(\vec{s}^{\,\ell}) \\
&\vdots \\
\vec{s}^{\,n-1} &= \vec{s}^{\,\ell} + a_{n-1} \Delta t\, F(\vec{s}^{\,n-2}) + b_{n-1} \Delta t\, F(\vec{s}^{\,n-3}) + c_{n-1} \Delta t\, F(\vec{s}^{\,n-4}) + \ldots \\
\vec{s}^{\,\ell+1} &= \vec{s}^{\,\ell} + a_n \Delta t\, F(\vec{s}^{\,n-1}) + b_n \Delta t\, F(\vec{s}^{\,n-2}) + c_n \Delta t\, F(\vec{s}^{\,n-3}) + \ldots
\end{aligned}\right\} \quad (2.7)$$

It is composed of n-1 predictor steps (the first n-1 steps) and 1 corrector step (the last step).
With a n-steps Runge-Kutta scheme, i.e. a Runge-Kutta scheme consisting of n steps, nth order accuracy in time can be obtained. A good accuracy in time is however not important when considering a steady flow problem. Important in that case is a fast convergence.

An improvement of the rate of convergence of (2.7) can be obtained by simplifying it to

$$\left.\begin{aligned}
&\vec{s}^{\,1} = \vec{s}^{\,l} + \Delta t\, F(\vec{s}^{\,l}) \\
&\vec{s}^{\,2} = \vec{s}^{\,l} + \Delta t\, F(\vec{s}^{\,1}) \\
&\vec{s}^{\,3} = \vec{s}^{\,l} + \Delta t\, F(\vec{s}^{\,2}) \\
&\quad\vdots \\
&\vec{s}^{\,n-1} = \vec{s}^{\,l} + \Delta t\, F(\vec{s}^{\,n-2}) \\
&\vec{s}^{\,l+1} = \vec{s}^{\,l} + a\Delta t\, F(\vec{s}^{\,n-1}) + b\Delta t\, F(\vec{s}^{\,n-2}) + c\Delta t\, F(\vec{s}^{\,n-3}) + \dots
\end{aligned}\right\} \quad (2.8)$$

The space operator F is composed of a convective and viscous operator;

$$F(\vec{s}) = C(\vec{s}) + V(\vec{s}) \qquad (2.9)$$

An improvement of the rate of convergence of (2.8) can now be obtained by simplifying it to

$$\left.\begin{aligned}
&\vec{s}^{\,1} = \vec{s}^{\,l} + \Delta t\{C(\vec{s}^{\,l}) + V(\vec{s}^{\,l})\} \\
&\vec{s}^{\,2} = \vec{s}^{\,l} + \Delta t\{C(\vec{s}^{\,1}) + V(\vec{s}^{\,l})\} \\
&\vec{s}^{\,3} = \vec{s}^{\,l} + \Delta t\{C(\vec{s}^{\,2}) + V(\vec{s}^{\,l})\} \\
&\quad\vdots \\
&\vec{s}^{\,n-1} = \vec{s}^{\,l} + \Delta t\{C(\vec{s}^{\,n-1}) + V(\vec{s}^{\,l})\} \\
&\vec{s}^{\,l+1} = \vec{s}^{\,l} + a\Delta t\{C(\vec{s}^{\,n-1}) + V(\vec{s}^{\,l})\} + b\Delta t\{C(\vec{s}^{\,n-2}) + V(\vec{s}^{\,l})\} + c\Delta t\{C(\vec{s}^{\,n-3}) + V(\vec{s}^{\,l})\} + \dots
\end{aligned}\right\} \quad (2.10)$$

, so by applying the viscous operator only in the first predictor step.

The time steps to be taken with the Runge-Kutta schemes are limited by stability requirements. Since a good accuracy in time is not important for steady flow problems, one does not need to take the same time step at each mesh point. Assuming that the larger the time steps taken, the better the rate of convergence, the best rate of convergence is obtained by taking at each mesh

point the maximum allowable time step.
For for instance the three-steps Runge-Kutta scheme which is third order accurate in time it holds: a=1/6, b=1/3 and c=1/2. Since a good accuracy in time is not important these coefficients may be changed such that a better rate of convergence is obtained. This now has been investigated for the Runge-Kutta schemes of the form (2.10) from n=2 up to and including n=6. The optimization of the coefficients has been performed numerically. The results obtained are given table 2.1.
From table 2.1 it appears that (theoretically) the four-steps Runge-Kutta scheme is the fastest scheme. The five-steps and six-steps Runge-Kutta schemes may be unstable when using them. The neutral stability curves of these schemes jump away from the origin at the left side of the imaginary axis. These schemes are therefore unstable for eigenvalues of the Navier-Stokes equations which have a very small real part.
The neutral stability curves belonging to the five Runge-Kutta schemes of table 2.1 are given in fig.2.2.

2.3. Stability analysis

In order to determine the eigenvalues λ of system (1.10) one can introduce

$$\begin{pmatrix} u \\ v \\ p \end{pmatrix} = \begin{pmatrix} U \\ V \\ P \end{pmatrix} e^{i(\omega_x x + \omega_y y)} \tag{2.11}$$

Substitution of (2.11) into (1.10) yields, written in matrix form

$$\begin{pmatrix} -ui\omega_x - vi\omega_y - \frac{1}{Re}(\omega_x^2+\omega_y^2) - \lambda & 0 & -i\omega_x \\ 0 & -ui\omega_x - vi\omega_y - \frac{1}{Re}(\omega_x^2+\omega_y^2) - \lambda & -i\omega_y \\ -bi\omega_x & -bi\omega_y & -\lambda \end{pmatrix} \begin{pmatrix} U \\ V \\ P \end{pmatrix} = 0 \tag{2.12}$$

A non-trivial solution $\begin{pmatrix} U \\ V \\ P \end{pmatrix}$ exists if the determinant of above matrix is zero, so if

$$\begin{vmatrix} a_1+\lambda & 0 & a_2 \\ 0 & a_1+\lambda & a_3 \\ a_2 b & a_3 b & \lambda \end{vmatrix} = 0 \tag{2.13}$$

with

$$\left.\begin{aligned} a_1 &= i(\omega_x u + \omega_y v) + \frac{1}{Re}(\omega_x^2 + \omega_y^2) \\ a_2 &= i\omega_x \\ a_3 &= i\omega_y \end{aligned}\right\} \quad (2.14)$$

From (2.13) it follows for the eigenvalues

$$\left.\begin{aligned} \lambda_1 &= -a_1 \\ \lambda_{2,3} &= \frac{-a_1 \pm \sqrt{a_1^2 + 4b(a_2^2 + a_3^2)}}{2} \end{aligned}\right\} \quad (2.15)$$

Substitution of (2.14) into (2.15) yields

$$\left.\begin{aligned} \lambda_1 &= -i(\omega_x u + \omega_y v) - \frac{1}{Re}(\omega_x^2 + \omega_y^2) \\ \lambda_{2,3} &= \frac{1}{2}\left[-i(\omega_x u + \omega_y v) - \frac{1}{Re}(\omega_x^2 + \omega_y^2) \pm \sqrt{\left\{i(\omega_x u + \omega_y v) + \frac{1}{Re}(\omega_x^2 + \omega_y^2)\right\}^2 - 4b(\omega_x^2 + \omega_y^2)}\right] \end{aligned}\right\} \quad (2.16)$$

Introducing

$$\left.\begin{aligned} \omega &= \sqrt{\omega_x^2 + \omega_y^2} \\ \cos\theta &= \frac{\omega_x}{\omega} \\ \sin\theta &= \frac{\omega_y}{\omega} \end{aligned}\right\} \quad (2.17)$$

we can write

$$\left.\begin{aligned} \lambda_1 &= -i\omega\left(u\cos\theta + v\sin\theta - i\frac{\omega}{Re}\right) \\ \lambda_{2,3} &= \frac{-i\omega}{2}\left[u\cos\theta + v\sin\theta - i\frac{\omega}{Re} \pm \sqrt{4b - \left\{i(u\cos\theta + v\sin\theta) + \frac{\omega}{Re}\right\}^2}\right] \end{aligned}\right\} \quad (2.18)$$

Using the relation

$$\lambda_j = -i\omega w_j \quad ; \quad j = 1, 2, 3 \qquad (2.19)$$

between the eigenvalues λ_j and the propagation speeds w_j one

obtains as expressions for the propagation speeds

$$\left.\begin{aligned} w_1 &= u\cos\theta + v\sin\theta - i\frac{\omega}{Re} \\ w_{2,3} &= \frac{1}{2}\left[u\cos\theta + v\sin\theta - i\frac{\omega}{Re} \pm \sqrt{4b - \left\{i\left(u\cos\theta + v\sin\theta\right) + \frac{\omega}{Re}\right\}^2}\right] \end{aligned}\right\} \quad (2.20)$$

These now are the expressions for the propagation speeds in the physical domain. The expressions need to be transformed to the computational domain. Denoting quantities in the computational domain with a bar, the relations to be used for the transformation are

$$\left.\begin{aligned} w &= \frac{\bar{w}}{\sqrt{\left(\frac{\cos\bar{\theta}}{x'}\right)^2 + \left(\frac{\sin\bar{\theta}}{y'}\right)^2}} \\ \cos\theta &= \frac{\cos\bar{\theta}/x'}{\sqrt{\left(\frac{\cos\bar{\theta}}{x'}\right)^2 + \left(\frac{\sin\bar{\theta}}{y'}\right)^2}} \\ \sin\theta &= \frac{\sin\bar{\theta}/y'}{\sqrt{\left(\frac{\cos\bar{\theta}}{x'}\right)^2 + \left(\frac{\sin\bar{\theta}}{y'}\right)^2}} \end{aligned}\right\} \quad (2.21)$$

in which $x' = \frac{dx}{d\bar{x}}$ and $y' = \frac{dy}{d\bar{y}}$.
With (2.21) obtained can be from (2.20)

$$\left.\begin{aligned} \bar{w}_1 &= u\frac{\cos\bar{\theta}}{x'} + v\frac{\sin\bar{\theta}}{y'} - i\frac{\omega}{Re}\sqrt{\left(\frac{\cos\bar{\theta}}{x'}\right)^2 + \left(\frac{\sin\bar{\theta}}{y'}\right)^2} \\ \bar{w}_{2,3} &= \frac{1}{2}\left[u\frac{\cos\bar{\theta}}{x'} + v\frac{\sin\bar{\theta}}{y'} - i\frac{\omega}{Re}\sqrt{\left(\frac{\cos\bar{\theta}}{x'}\right)^2 + \left(\frac{\sin\bar{\theta}}{y'}\right)^2} + \right. \\ &\quad \left. \pm\sqrt{4b\left\{\left(\frac{\cos\bar{\theta}}{x'}\right)^2 + \left(\frac{\sin\bar{\theta}}{y'}\right)^2\right\} - \left\{i\left(u\frac{\cos\bar{\theta}}{x'} + v\frac{\sin\bar{\theta}}{y'}\right) + \frac{\omega}{Re}\sqrt{\left(\frac{\cos\bar{\theta}}{x'}\right)^2 + \left(\frac{\sin\bar{\theta}}{y'}\right)^2}\right\}^2}\right] \end{aligned}\right\} \quad (2.22)$$

For the discretized problem in the computational domain introduced then has to be

$$\left.\begin{aligned} \cos\bar{\theta} &= \frac{\sin k_1/\Delta\bar{x}}{\sqrt{\left(\frac{\sin k_1}{\Delta\bar{x}}\right)^2 + \left(\frac{\sin k_2}{\Delta\bar{y}}\right)^2}} \\ \sin\bar{\theta} &= \frac{\sin k_2/\Delta\bar{y}}{\sqrt{\left(\frac{\sin k_1}{\Delta\bar{x}}\right)^2 + \left(\frac{\sin k_2}{\Delta\bar{y}}\right)^2}} \end{aligned}\right\} \quad (2.23)$$

For the eigenvalues $\bar{\lambda}_j$ of the discretized problem in the computational domain it holds

$$\bar{\lambda}_j = -i\sqrt{\left(\frac{\sin k_1}{\Delta\bar{x}}\right)^2 + \left(\frac{\sin k_2}{\Delta\bar{y}}\right)^2}\,\bar{w}_j \quad ; \quad j = 1,2,3 \qquad (2.24)$$

Using (2.23) and (2.24) one obtains finally as expressions for the

eigenvalues $\bar{\lambda}_j$ of the discretized problem in the computational domain

$$\left.\begin{aligned}
\bar{\lambda}_1 &= -i\left(u\frac{\sin k_1}{\Delta\bar{x}x'} + v\frac{\sin k_2}{\Delta\bar{y}y'}\right) - \frac{1}{Re}\sqrt{\left(\frac{\sin k_1}{\Delta\bar{x}}\right)^2+\left(\frac{\sin k_2}{\Delta\bar{y}}\right)^2}\sqrt{\left(\frac{\sin k_1}{\Delta\bar{x}x'}\right)^2+\left(\frac{\sin k_2}{\Delta\bar{y}y'}\right)^2} \\
\bar{\lambda}_{2,3} &= \frac{1}{2}\left[-i\left(u\frac{\sin k_1}{\Delta\bar{x}x'} + v\frac{\sin k_2}{\Delta\bar{y}y'}\right) - \frac{1}{Re}\sqrt{\left(\frac{\sin k_1}{\Delta\bar{x}}\right)^2+\left(\frac{\sin k_2}{\Delta\bar{y}}\right)^2}\sqrt{\left(\frac{\sin k_1}{\Delta\bar{x}x'}\right)^2+\left(\frac{\sin k_2}{\Delta\bar{y}y'}\right)^2} + \right. \\
&\left. \pm\sqrt{\left\{i\left(u\frac{\sin k_1}{\Delta\bar{x}x'}+v\frac{\sin k_2}{\Delta\bar{y}y'}\right)+\frac{1}{Re}\sqrt{\left(\frac{\sin k_1}{\Delta\bar{x}}\right)^2+\left(\frac{\sin k_2}{\Delta\bar{y}}\right)^2}\sqrt{\left(\frac{\sin k_1}{\Delta\bar{x}x'}\right)^2+\left(\frac{\sin k_2}{\Delta\bar{y}y'}\right)^2}\right\}^2 - 4b\left\{\left(\frac{\sin k_1}{\Delta\bar{x}x'}\right)^2+\left(\frac{\sin k_2}{\Delta\bar{y}y'}\right)^2\right\}}\right]
\end{aligned}\right\} \quad (2.25)$$

Most critical for the stability are the modes with wave numbers $k_1=k_2=\frac{\pi}{2}$. From (2.25) it follows

$$\left.\begin{aligned}
(\bar{\lambda}_1)_{k_1=k_2=\frac{\pi}{2}} &= -i\left(\frac{u}{\Delta\bar{x}x'}+\frac{v}{\Delta\bar{y}y'}\right) - \frac{1}{Re}\sqrt{\left(\frac{1}{\Delta\bar{x}}\right)^2+\left(\frac{1}{\Delta\bar{y}}\right)^2}\sqrt{\left(\frac{1}{\Delta\bar{x}x'}\right)^2+\left(\frac{1}{\Delta\bar{y}y'}\right)^2} \\
(\bar{\lambda}_{2,3})_{k_1=k_2=\frac{\pi}{2}} &= \frac{1}{2}\left[-i\left(\frac{u}{\Delta\bar{x}x'}+\frac{v}{\Delta\bar{y}y'}\right) - \frac{1}{Re}\sqrt{\left(\frac{1}{\Delta\bar{x}}\right)^2+\left(\frac{1}{\Delta\bar{y}}\right)^2}\sqrt{\left(\frac{1}{\Delta\bar{x}x'}\right)^2+\left(\frac{1}{\Delta\bar{y}y'}\right)^2} + \right. \\
&\left. \pm\sqrt{\left\{i\left(\frac{u}{\Delta\bar{x}x'}+\frac{v}{\Delta\bar{y}y'}\right)+\frac{1}{Re}\sqrt{\left(\frac{1}{\Delta\bar{x}}\right)^2+\left(\frac{1}{\Delta\bar{y}}\right)^2}\sqrt{\left(\frac{1}{\Delta\bar{x}x'}\right)^2+\left(\frac{1}{\Delta\bar{y}y'}\right)^2}\right\}^2 - 4b\left\{\left(\frac{1}{\Delta\bar{x}x'}\right)^2+\left(\frac{1}{\Delta\bar{y}y'}\right)^2\right\}}\right]
\end{aligned}\right\} \quad (2.26)$$

The maximum allowable time step to be taken now in each mesh point is limited by the $(\bar{\lambda}_j)_{k_1=k_2=\frac{\pi}{2}}$ with the largest modulus in that mesh point. The time step to be made should satisfy

$$\Delta t \leq \frac{|r|_{RK}}{|\bar{\lambda}_j|_{max,\,k_1=k_2=\frac{\pi}{2}}} \quad (2.27)$$

in which $|r|_{RK}$ is the radius of the neutral stability curve of the considered Runge-Kutta scheme, for the argument corresponding with $|\bar{\lambda}_j|_{max,k_1=k_2=\frac{\pi}{2}}$. Inequality (2.27) comes from a von Neumann stability analysis, so an analysis which is not valid for non-linear problems. Assumed now is that for the destabilizing effect of non-linearities can be accounted by simply introducing a safety factor into (2.27), so by satisfying

$$\Delta t \leq sfact\ \frac{|r|_{RK}}{|\bar{\lambda}_j|_{max,\,k_1=k_2=\frac{\pi}{2}}} \quad (2.28)$$

with sfact<1.

2.4. Boundary conditions

As physical boundary conditions have been used:

- at all walls

$$\left.\begin{aligned} u &= 0 \\ v &= 0 \end{aligned}\right\} \quad (2.29)$$

- at the inlet the Poiseuille solution for the velocity in the inlet part, so

$$\left.\begin{aligned} u &= \frac{-4}{(y_{upper} - y_{step})^2}(y - y_{step})(y - y_{upper}) \\ v &= 0 \end{aligned}\right\} \quad (2.30)$$

- and at the outlet

$$p = 0 \quad (2.31)$$

As numerical boundary conditions have been used:

- at the horizontal walls

$$\frac{\partial p}{\partial y} = \frac{1}{Re}\frac{\partial^2 v}{\partial y^2} \quad (2.32)$$

- at the vertical wall of the step

$$\frac{\partial p}{\partial x} = \frac{1}{Re}\frac{\partial^2 u}{\partial x^2} \quad (2.33)$$

- at the inlet

$$\frac{\partial^2 p}{\partial x^2} = 0 \quad (2.34)$$

- and at the outlet

$$\left.\begin{aligned} \frac{\partial u}{\partial x} &= 0 \\ \frac{\partial v}{\partial x} &= 0 \end{aligned}\right\} \quad (2.35)$$

The numerical boundary condition at all walls is the momentum equation normal to the corresponding wall.

The numerical boundary condition at the inlet and outlet come from the Poiseuille solution.

For the numerical boundary condition at the convex and concave corner of the step, use has been made of

$$cvx\frac{\partial p}{\partial x} + cvy\frac{\partial p}{\partial y} = \frac{1}{Re}\left(\frac{\partial^2 u}{\partial x^2} + \frac{\partial^2 v}{\partial y^2}\right) \tag{2.36}$$

respectively

$$ccx\frac{\partial p}{\partial x} + ccy\frac{\partial p}{\partial y} = 0 \tag{2.37}$$

in which cvx, cvy, ccx and ccy are weight coefficients.

The boundary conditions are summarized in fig.2.3.

2.5. Initial solution

As initial solution has been used in both the inlet and outlet part; the corresponding Poiseuille solution. Both solutions are related with each other by the law of conservation of mass.
In order to be consistent with the boundary condition for the pressure at the outlet the initial pressure has been taken equal to zero at the outlet.
So the initial solution used in the inlet part is

$$\left.\begin{aligned} u &= \frac{-4}{(y_{upper1}-y_{step})^2}(y-y_{step})(y-y_{upper1}) \\ v &= 0 \\ p &= \frac{-8}{Re\,(y_{upper1}-y_{step})^2}\left\{x - \left(\frac{y_{upper1}-y_{step}}{y_{upper1}}\right)^3 x_{outlet}\right\} \end{aligned}\right\} \tag{2.38}$$

, and the initial solution used in the outlet part is

$$\left.\begin{aligned} u &= \frac{-4\,(y_{upper1}-y_{step})}{y_{upper1}^3}\,y\,(y-y_{upper1}) \\ v &= 0 \\ p &= \frac{-8\,(y_{upper1}-y_{step})}{Re\,y_{upper1}^3}\,(x-x_{outlet}) \end{aligned}\right\} \tag{2.39}$$

For a channel of which the step has the same height as the inlet part and for Re=50, the initial solution is given in fig.2.4. The pressure distribution given in fig.2.4b is the pressure difference $Re\{p(m,j)-p(m_{step},j_{step})\}$.

The initial solution is physically unrealistic; no separation occurs at the convex corner of the step.

2.6. Convergence test

For the convergence test considered has been after each time step, i.e. after each iteration with the Runge-Kutta scheme: the maximum value for all (inner) mesh points of $\frac{\partial s_j}{\partial t}$; j=1,2,3. As convergence criterion has now been used that as soon as this maximum is lower than 10^{-6} the steady state has been reached; i.e. the iteration procedure has converged.

2.7. Computer program

A global flow chart of the computer program has been given in fig.2.5.
For getting a (converged) solution the first four blocks in the flow chart are of course important but need taken together less than 0.1 percent of the CPU TIME needed by both loops taken together.
From the inner loop in fig.2.5 it appears that the boundary conditions are imposed not only after the corrector step, but after each predictor step.
After having performed the inner loop, the convergence to the steady state is investigated at all inner mesh points. Because $\frac{\Delta s_j}{\Delta t}$ is considered for the convergence test and because Δt is not known for the points on the boundaries, only the inner points can be considered for the convergence test. If the convergence test is not satisfied for all inner mesh points a return is made; the maximum allowable time step to be made in each inner mesh point is computed again, making use of the latest solution, and new time steps are made. As soon as the convergence test is satisfied at all inner mesh points, the outer loop will be left, i.e. the solution will have been obtained.

3. RESULTS

3.1. Test cases

Two different geometries have been considered for the channel with step;
- a channel with an inlet which has the same height as the step (channel with small inlet), and
- a channel with an inlet which is twice as high as the step (channel with big inlet).

The length of the inlet and outlet part of both channels is the same. Both channels are given in fig.3.1.

In both channels the flow has been computed for Re=50.

The mesh used for both test cases is given in table 3.1 and fig.3.2. As appears from table 3.1 and fig.3.2, both meshes are slightly stretched.

For both test cases as safety factor on the time steps made has been used: sfact=0.9. Divergence occurred for sfact$\geq$0.95.

3.2. Convergence history

The convergence history obtained for both test cases on the VAX 11/780 is given in fig.3.3.

For both test cases use has been made of a four-steps Runge-Kutta scheme. In practice it also appeared that this scheme gives the best rate of convergence. To proof this the flow in the channel with small inlet has been computed for Re=50, using two different two-steps Runge-Kutta schemes, and one three-steps and one four-steps Runge-Kutta scheme. The input parameters and convergence characteristics of these four Runge-Kutta schemes are given in table 3.2. The two-steps Runge-Kutta scheme with sfact=$\frac{1}{2}\sqrt{2}$ has been considered because it has recently appeared from theory that $\frac{1}{2}\sqrt{2}$ times the maximum allowable time steps might give the best rate of convergence obtainable with a two-steps Runge-Kutta

scheme.
So it appears from table 3.2 that the four-steps Runge-Kutta scheme gives the fastest convergence to the steady state.

For both test cases use has been made of b=0.5. It has appeared that this value of b gives the best rate of convergence.

For the channel with big inlet the rate of convergence is better than for the channel with small inlet. After 60 minutes of CPU TIME the value of $\left(\frac{\partial s}{\partial t}\right)_{max}$ for the channel with small and big inlet is equal to 10^{-4} respectively 10^{-5}. The difference between these two values is too large to have been caused by the somewhat smaller number of points in the channel with big inlet.

In table 3.3 a comparison has been made between the present CPU TIMES needed to converge to the steady state and the same CPU TIMES as needed by some contributors to the GAMM Workshop. The CPU TIMES of the contributors to the GAMM Workshop have been corrected for the difference in computer used. The CPU TIMES given in table 3.3 are the CPU TIMES needed to converge to the steady state, when making use of the VAX 11/780.
The present CPU TIMES are nearly the same as those of two of the contributors in table 3.3.

To illustrate the large values of $\left(\frac{\partial s}{\partial t}\right)_{max}$ occurring in the beginning of the time-marching procedure and the convergence to the steady state, given are in fig.3.4 for the channel with small inlet and Re=50: for several iteration levels; the streamline distribution in the neighbourhood of the step and the velocity profile at the location which will finally become the location of the reattachment point.
In the convergence history at the left of each streamline distribution the corresponding iteration level has been indicated.
Clearly visible are the large changes in the streamline distribution, occurring at large values of $\left(\frac{\partial s}{\partial t}\right)_{max}$ in the beginning of the convergence history.
Hardly visible are the changes in the streamline distribution occuring at the end of the convergence history, and with that clearly visible is: the convergence to the steady state.

3.3. Streamline distribution and velocity profiles

The streamline distribution obtained for both test cases is given (for the entire integration regions) in fig.3.5.
In fig.3.6 and 3.7 the streamline distributions are given in more detail and with some velocity profiles added to it.

The velocity profile in the inlet part and the velocity profile downstream of the reattachment point are for both test cases by very good approximation equal to the corresponding Poiseuille velocity profile.
Concerning the other velocity profiles; the velocity profile at the reattachment point has in agreement with the physics a slope $\frac{du}{dy}=0$ at the wall, and the velocity profile at the vortex center has in agreement with the physics: u=0 in the vortex center.

For both test cases a comparison has been made with the results obtained at VKI by Borsboom for exactly the same test cases (but with the compressible Navier-Stokes equations and a finite volume discretization).
The agreement between both present streamline distributions and those of Borsboom is reasonably good. In both cases nearly the same values have been obtained for the stream function $\psi=\int\int(udy-vdx)dxdy$. The only difference between the present streamline distributions and those obtained by Borsboom appears in the test case of the channel with small inlet, and concerns the location of the reattachment point. In the present results, for the channel with small inlet the reattachment point is located further upstream than in the results of Borsboom.

The choice of the weight coefficients cvx and cvy has hardly any influence on the location of the reattachment point. For both test cases used has been: cvx=cvy=0.5.

Remarkable is that for both test cases the x-coordinate of the vortex center is exactly 3 times smaller than the x-coordinate of the reattachment point.

In table 3.4 a comparison has been made between
- the present locations of the reattachment point and those obtained by the persons already mentioned in table 3.3, and between
- the maximum velocity component in x-direction at the location x=0.8 and that obtained by the other persons.

The agreement between the present results and those obtained by the others is better for the channel with big inlet than for the channel with small inlet.

3.4. Pressure distribution

The pressure distribution obtained for both test cases is given (for the entire integration regions) in fig.3.8.
Just as in fig.2.4b plotted has been the pressure difference $Re\{p(m,j)-p(m_{step},j_{step})\}$.

As can be seen in both fig.3.8a and 3.8b the pressure is wiggled in the neighbourhood of the step.
In order to remove the wiggles use has been made of several combinations of numerical boundary conditions and several different meshes.

For the numerical boundary conditions at the walls, use has been made of:

- the inviscid momentum equation normal to the corresponding wall;

$$\frac{\partial p}{\partial n}=0 \qquad (3.1)$$

- and the viscous momentum equation normal to the corresponding wall;

$$\frac{\partial p}{\partial n}=\frac{1}{Re}\frac{\partial^2 u_n}{\partial n^2} \qquad (3.2)$$

For the numerical boundary condition for the pressure at the inlet, use has been made of:

- the unsteady continuity equation;

$$\frac{\partial p}{\partial t} = -b\frac{\partial u}{\partial x} \tag{3.3}$$

- the steady momentum equation in x-direction;

$$\frac{\partial^2 p}{\partial x^2} = 0 \tag{3.4}$$

- and the "upstream characteristic relation" belonging to the system

$$\left.\begin{aligned} &\frac{\partial p}{\partial t} + b\frac{\partial u}{\partial x} = 0 \\ &\frac{\partial u}{\partial t} + \frac{\partial p}{\partial x} = \frac{-8}{Re\,(y_{upper} - y_{step})^2} \end{aligned}\right\} \tag{3.5}$$

For the numerical boundary condition for u at the outlet, use has only been made of the continuity equation;

$$\frac{\partial u}{\partial x} = 0 \tag{3.6}$$

The momentum equation in x-direction has not been used. This because u cannot be obtained explicitly from that equation in an easy way.

For the numerical boundary condition for v at the outlet, use has been made of:

- the steady momentum equation in y-direction;

$$\frac{\partial v}{\partial x} = 0 \tag{3.7}$$

- and the unsteady momentum equation in y-direction;

$$\frac{\partial v}{\partial t} + u\frac{\partial v}{\partial x} = 0 \tag{3.8}$$

It has appeared that of the previous numerical boundary conditions only that for the pressure at the inlet has influence on the smoothness of the solution. It has appeared that use of the numerical boundary condition $\frac{\partial^2 p}{\partial x^2}=0$ at the inlet gives the

smoothest solution.

For the numerical boundary condition for the pressure at the convex corner of the step use has been made of both

$$cvx\frac{\partial p}{\partial x} + cvy\frac{\partial p}{\partial y} = 0 \qquad (3.9)$$

and

$$cvx\frac{\partial p}{\partial x} + cvy\frac{\partial p}{\partial y} = \frac{1}{Re}\left(\frac{\partial^2 u}{\partial x^2} + \frac{\partial^2 v}{\partial y^2}\right) \qquad (3.10)$$

It has appeared that neither the choice of the weight coefficients cvx and cvy nor the use of (3.9) or (3.10) has some influence on the smoothness of the solution.

Smoothed and in more detail the pressure distribution is given in fig.3.9 and 3.10. (The smoothing applied is nothing else but a summation of the pressure and coordinates of the 4 neighbouring mesh points (m,j), (m+1,j), (m,j+1) and (m+1,j+1), and next a dividing by 4.)

For both test cases a comparison has been made again with Borsboom. Borsboom's pressure distribution in the neighbourhood of the step is smoother and has larger gradients. This might be due to the fact that Borsboom uses a mesh which is much finer in the neighbourhood of the step and moreover better adapted to the streamline distribution in the neighbourhood of the step (fig.3.11).
It has appeared that the coarser the mesh, the larger the wiggles, and also the further extended the wiggles. For the channel with small inlet a mesh which was twice as fine in both x- and y-direction as that given in fig.3.2a gave however no improvements. Maybe this finer mesh was not yet fine enough, or maybe it is the not-being well-adapted of the mesh to the streamline distribution which causes for the greater part the (last) wiggles.

3.5. Higher Reynolds number flows

Flows at higher Reynolds numbers have been considered as well. No convergence to the steady state has been obtained (for both the

channel with small and big inlet) for Re≥150. For the channel with small inlet the divergence history obtained for Re=150 and Re=500 is given in fig.3.12. For both high Reynolds number cases all input parameters (except of course Re) were the same as those used for the test case with Re=50.
Several possible changes have been tried separately and in combination in order to avoid the divergence; lowering of the safety factor, use of two-steps and three-steps Runge-Kutta schemes, application of the viscous operator in each predictor step, and decreasing of the stretching of the mesh. No remedy has been found. Remarkable was that the effect of lowering the safety factor with a certain factor just led to an increase with the same factor of the time after which divergence occurred.

3.6. Channel with cavity

In order to show that the computer program can be modified for the computation of flows in other geometries, computed has been the flow in a channel with cavity.
As initial solution in the channel has been used: the Poiseuille solution for that channel, and in the cavity: no flow at all but the same pressure distribution as in the part of the channel above it. The initial streamline distribution and the initial velocity profile at the center of the cavity are given in fig.3.13a.
The converged streamline distribution and the converged velocity profile are given in fig.3.13b. In more detail the latter streamline distribution and velocity profile are given in fig.3.13c.

4. CONCLUSIONS

The computational results are in agreement with the expected physical results.

The computational results are in reasonably good agreement with the computational results of others.

The rates of convergence obtained are nearly the same as those obtained by some contributors to the GAMM Workshop.
The best rate of convergence is obtained with a four-steps Runge-Kutta scheme.

The smoothness of the solution is strongly dependent on the numerical boundary condition for the pressure at the inlet.
The smoothest solution is obtained with a zero second order derivative of the pressure, normal to the inlet.

5. RECOMMENDATIONS

Before making the step to the computation of more complicated flows such as 3-dimensional, compressible or turbulent flows, the capability to compute higher Reynolds number flows should be improved.
A way of improving this capability is to artificially add viscosity, taking care for the accuracy of the solution.

Once one succeeds in computing higher Reynolds number flows an urgent demand for a faster convergence might still exist. Before making the step to more complicated flows this demand should be met. In order to further increase the rate of convergence, investigated could for instance be if an implicit scheme exists which is much faster than the four-steps Runge-Kutta scheme, and if a multigrid technique can be applied to that scheme.

6. REFERENCES

1. Numerical Solution of Incompressible Flow Problems.
   Chorin, A.J.
   Studies in Numerical Analysis 2, p. 64-71 (1968).

2. Numerical Analysis of Laminar Flow over a Step.
   Reunion/INRIA/Workshop.
   Bièvres, 1983.

table 2.1: Results optimization Runge-Kutta schemes

Runge-Kutta scheme	a	b	c	d	e	f	(rate of conv. RKi)/ (rate of conv. explicit MacCormack)	remarks
two-steps (RK2)	1	0	-	-	-	-	1.33	-
three-steps (RK3)	1/6	1/3	1/2	-	-	-	2.00	-
four-steps (RK4)	1/24	1/8	1/3	1/2	-	-	2.26	-
five-steps (RK5)	1/120	1/30	1/8	1/3	1/2	-	-	unstable for eigenvalues with a small real part
six-steps (RK6)	1/720	1/144	1/30	1/8	1/3	1/2	-	

table 3.1a: x-coordinates mesh for both channel with small and big inlet

-6.00	0.21
-5.39	0.44
-4.82	0.70
-4.28	0.98
-3.78	1.29
-3.31	1.64
-2.87	2.02
-2.46	2.44
-2.08	2.91
-1.72	3.42
-1.38	3.99
-1.07	4.62
-0.77	5.31
-0.50	6.08
-0.24	6.93
0.00	7.87
	8.91
	10.05
	11.32
	12.72
	14.27
	15.98
	17.87
	19.96
	22.26
	24.82
	27.64
	30.75
	34.19
	38.00

table 3.1b: y-coordinates mesh

channel with small inlet	channel with big inlet
2.00	3.00
1.92	2.87
1.83	2.72
1.73	2.56
1.62	2.39
1.50	2.20
1.38	2.00
1.27	1.80
1.17	1.61
1.08	1.44
1.00	1.28
0.92	1.13
0.83	1.00
0.73	0.86
0.62	0.70
0.50	0.50
0.38	0.30
0.27	0.14
0.17	0.00
0.08	
0.00	

table 3.2: Input parameters and convergence characteristics Runge-Kutta schemes

Runge-Kutta scheme	sfact	a	b	c	d	converged?	CPU TIME used (min.)
two-steps	0.90	1	0	-	-	no	150
two-steps	$\frac{1}{2}\sqrt{2}$	1	0	-	-	no	150
three-steps	0.90	1/6	1/3	1/2	-	yes	150
four-steps	0.90	1/24	1/8	1/3	1/2	yes	100

table 3.3: CPU TIMES (min.) needed on the VAX 11/780 for convergence to the steady state

	channel with small inlet, Re=50	channel with big inlet, Re=50
present method	100	70
Becker	14	14
Brédif	27	20
Nicolai and Pironneau	105	77
Ecer, a.o.	1020	1680
Wilkes, a.o.	129	83

table 3.4: Location reattachment point and maximum velocity component in x-direction at x=0.8

	channel with small inlet		channel with big inlet	
	$x_{reatt.\ point}$	u_{max} at x=0.8	$x_{reatt.\ point}$	u_{max} at x=0.8
present method	2.8	0.88	2.7	0.92
Becker	4.0	0.85	2.7	0.94
Brédif	2.1	0.73	2.9	0.90
Nicolai and Pironneau	2.3	-	3.0	-
Ecer, a.o.	0.6	0.61	1.2	0.82
Wilkes, a.o.	2.0	0.72	3.0	0.91

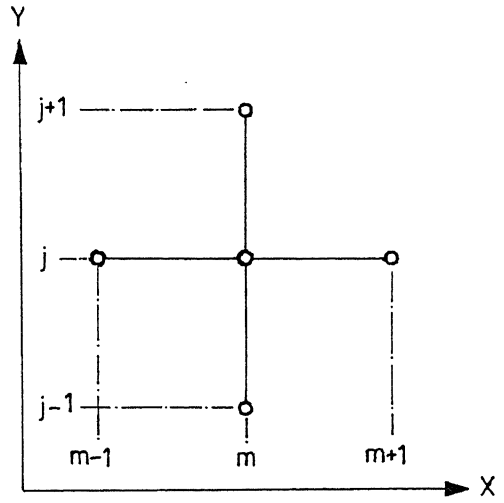

fig.1.1: Five-points scheme

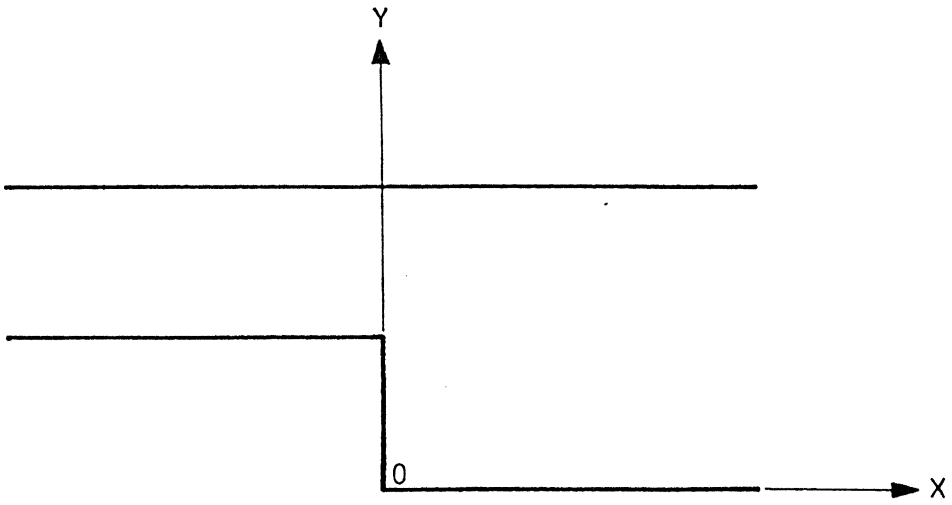

fig.2.1: Coordinate system in physical domain

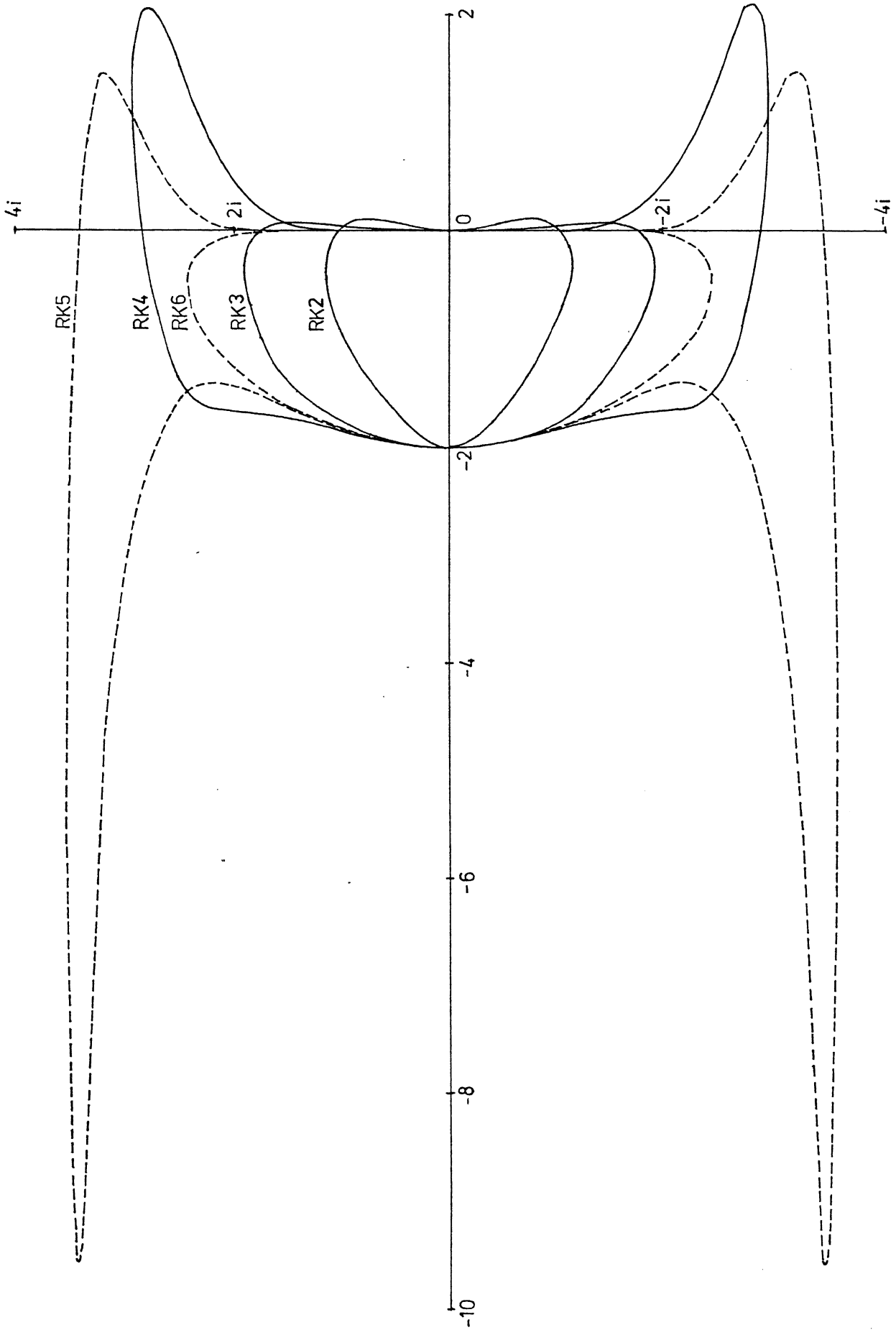

fig.2.2: Neutral stability curves Runge-Kutta schemes

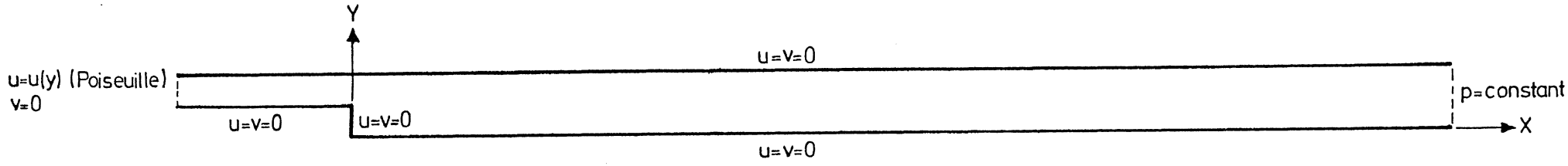

fig.2.3a: Physical boundary conditions

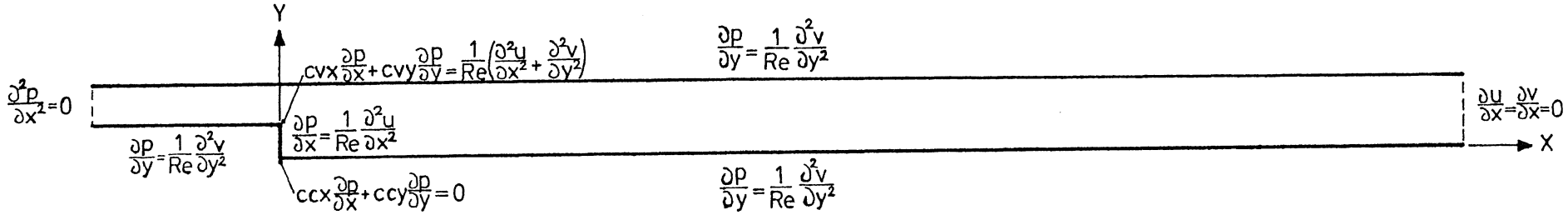

fig.2.3b: Numerical boundary conditions

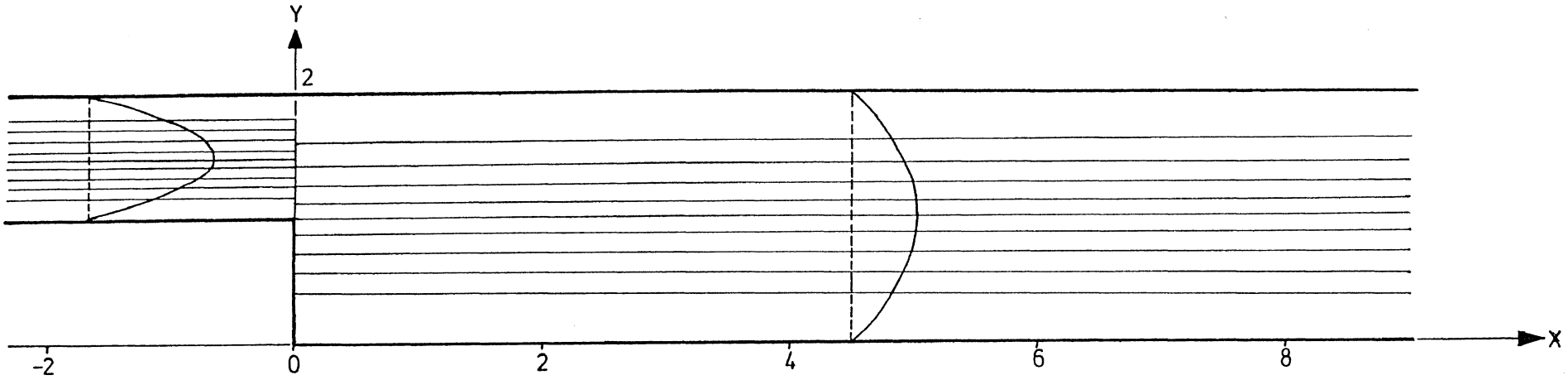

fig.2.4a: Initial streamline distribution

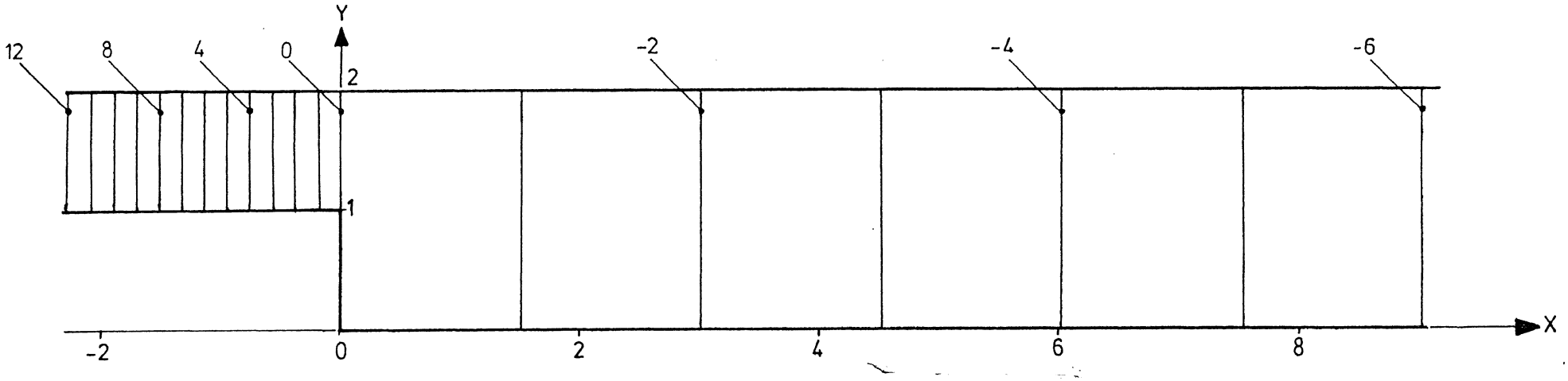

fig.2.4b: Initial pressure distribution; Re=50

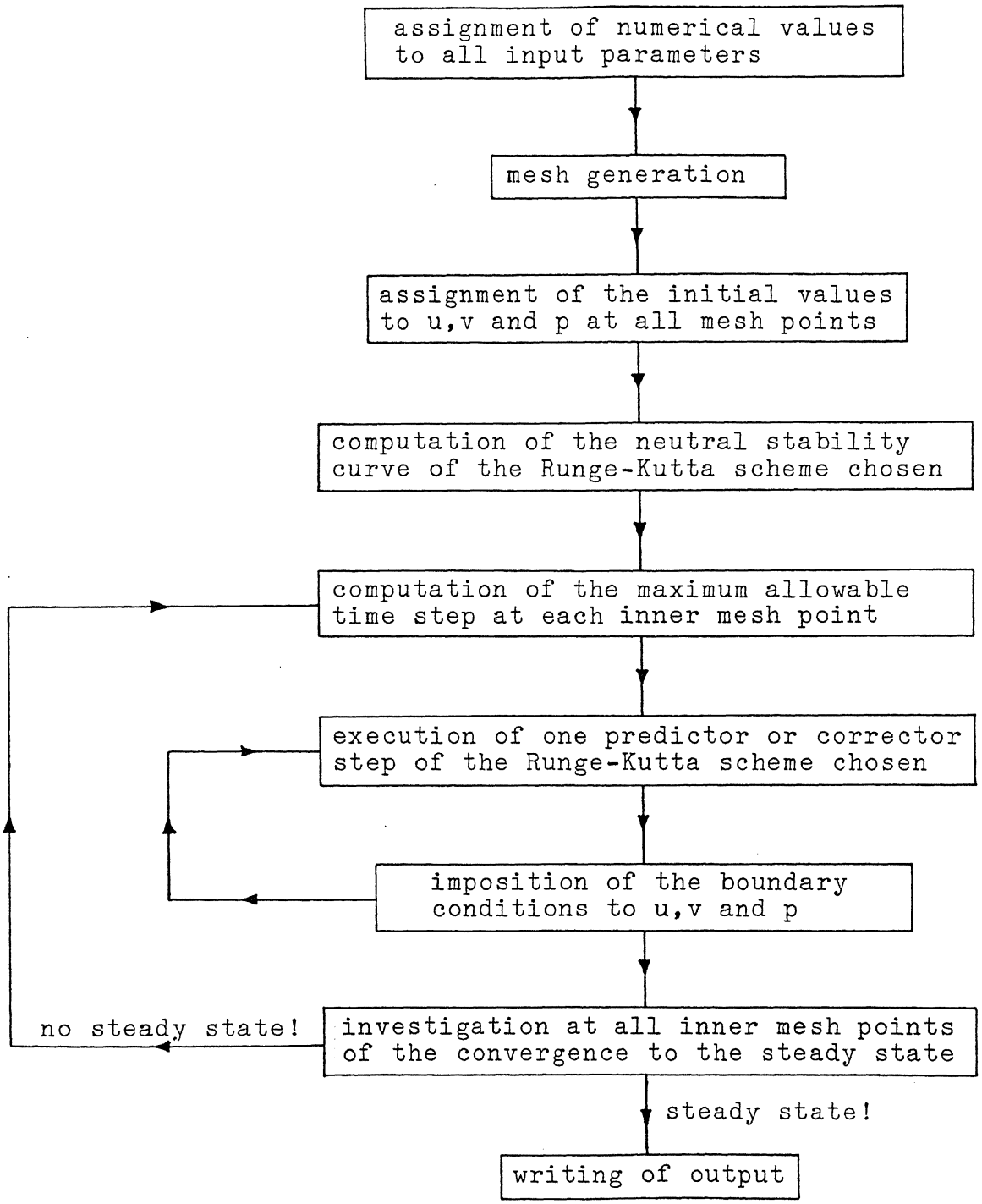

fig.2.5: Flow chart computer program

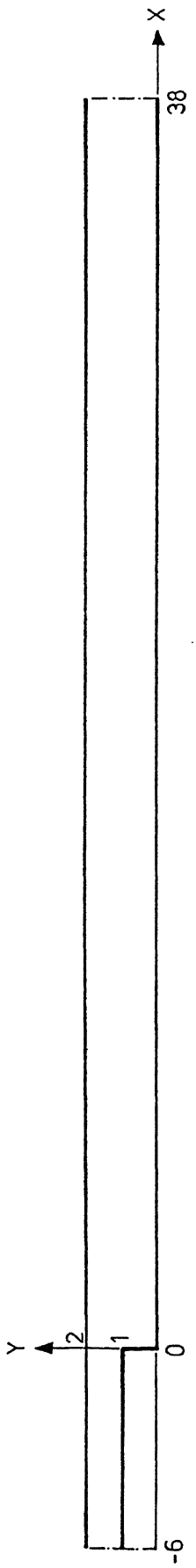

fig.3.1a: Channel with small inlet

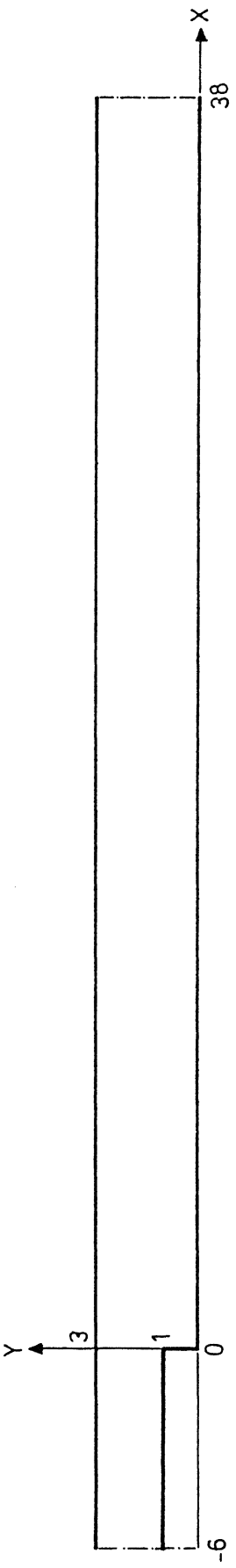

fig.3.1b: Channel with big inlet

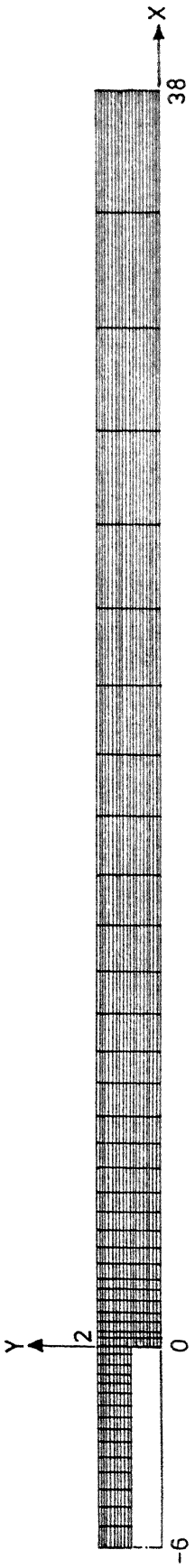

fig.3.2a: Mesh channel with small inlet

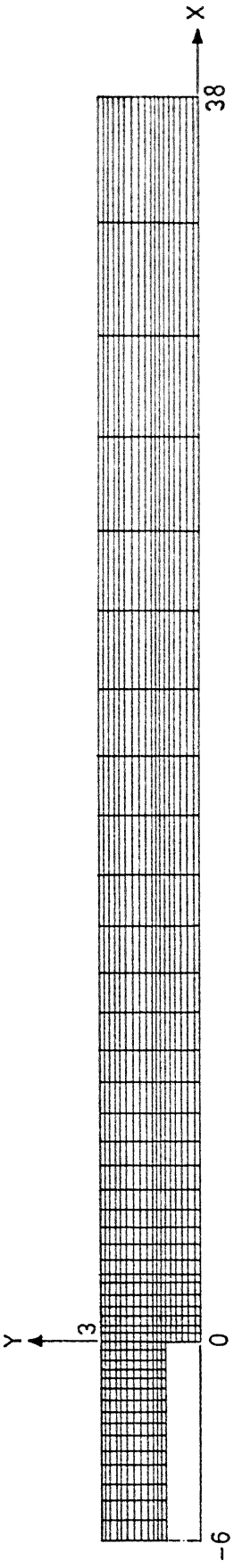

fig.3.2b: Mesh channel with big inlet

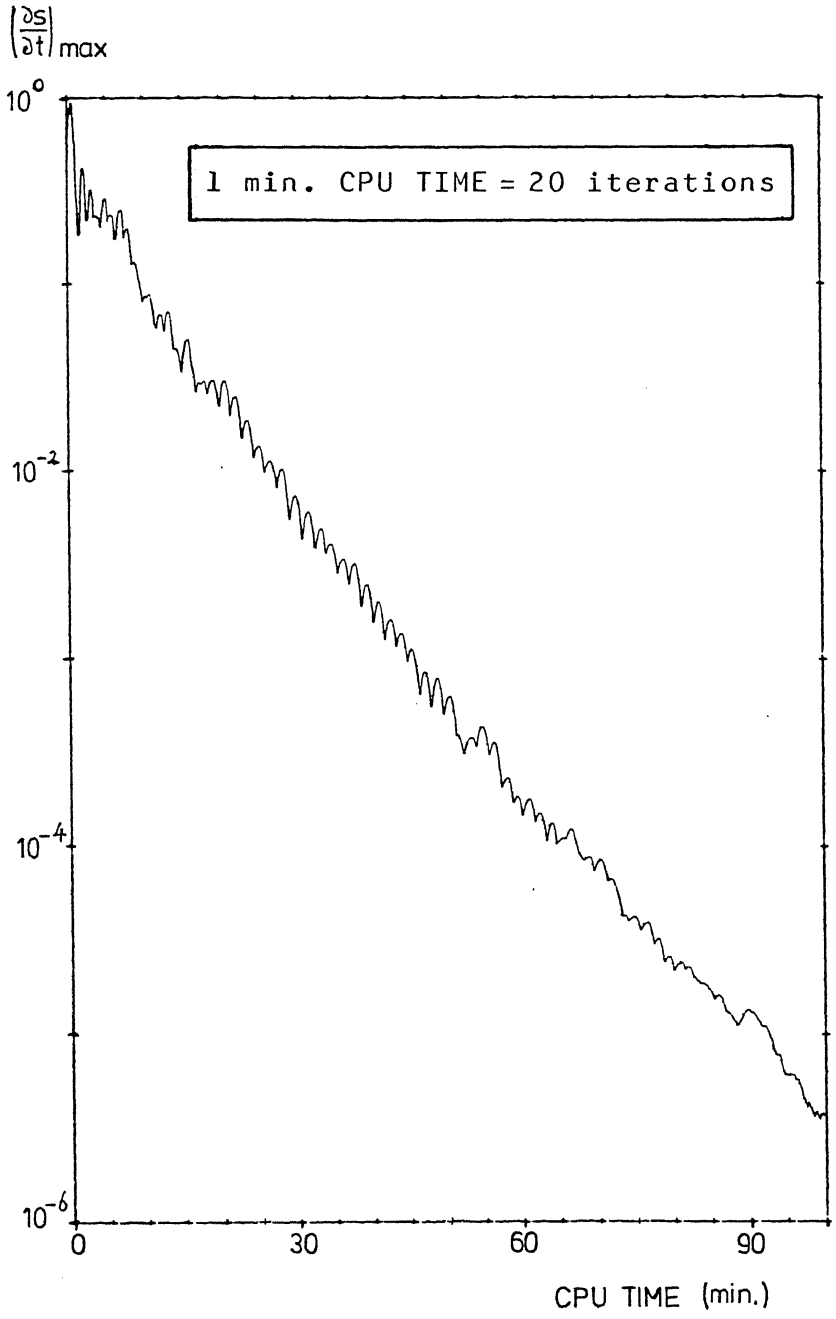

fig.3.3a: Convergence history; channel with small inlet, Re=50

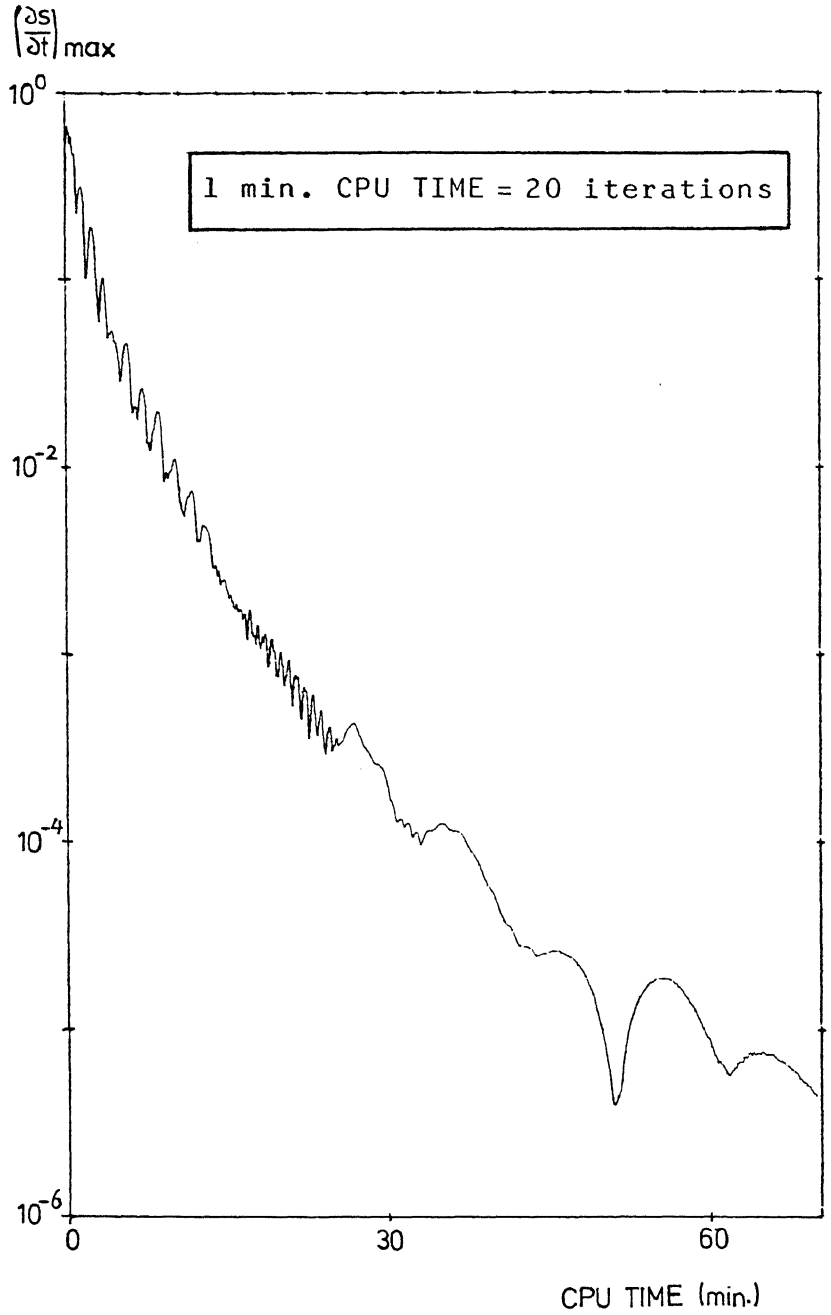

fig.3.3b: Convergence history; channel with big inlet, Re=50

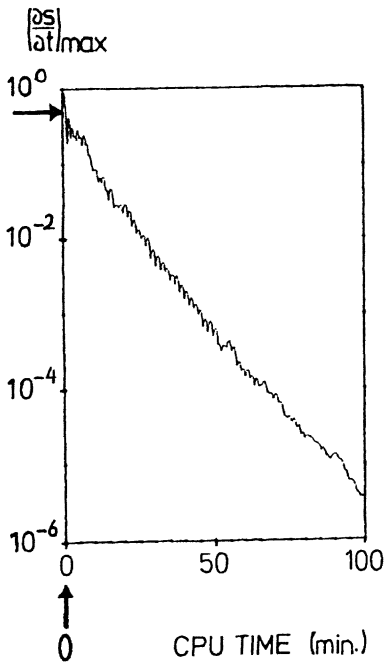

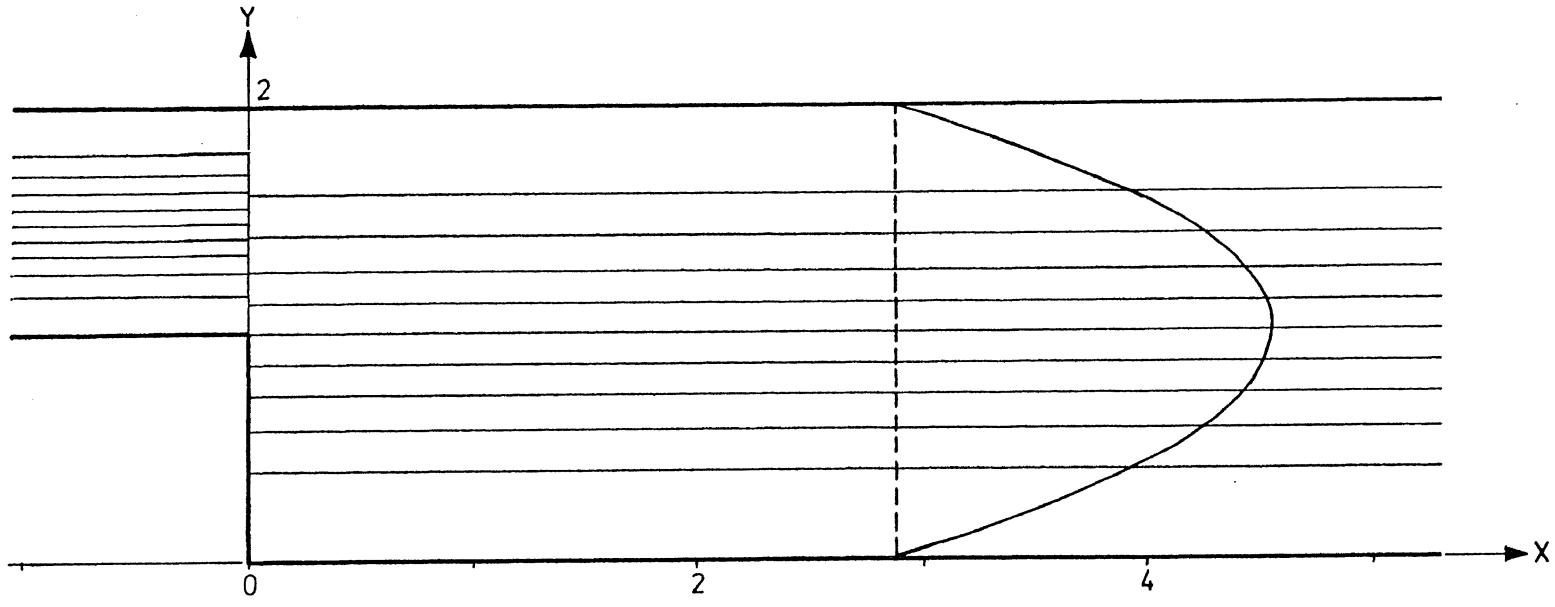

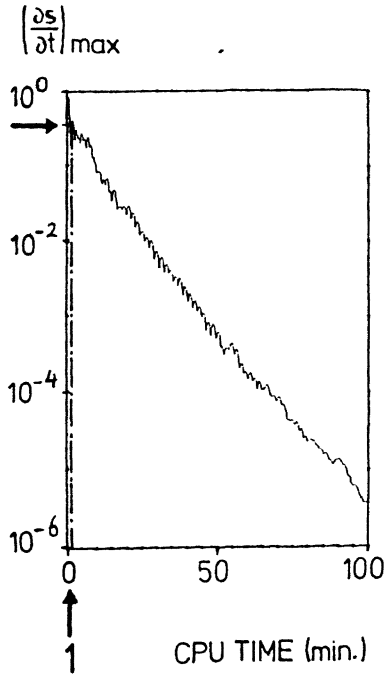

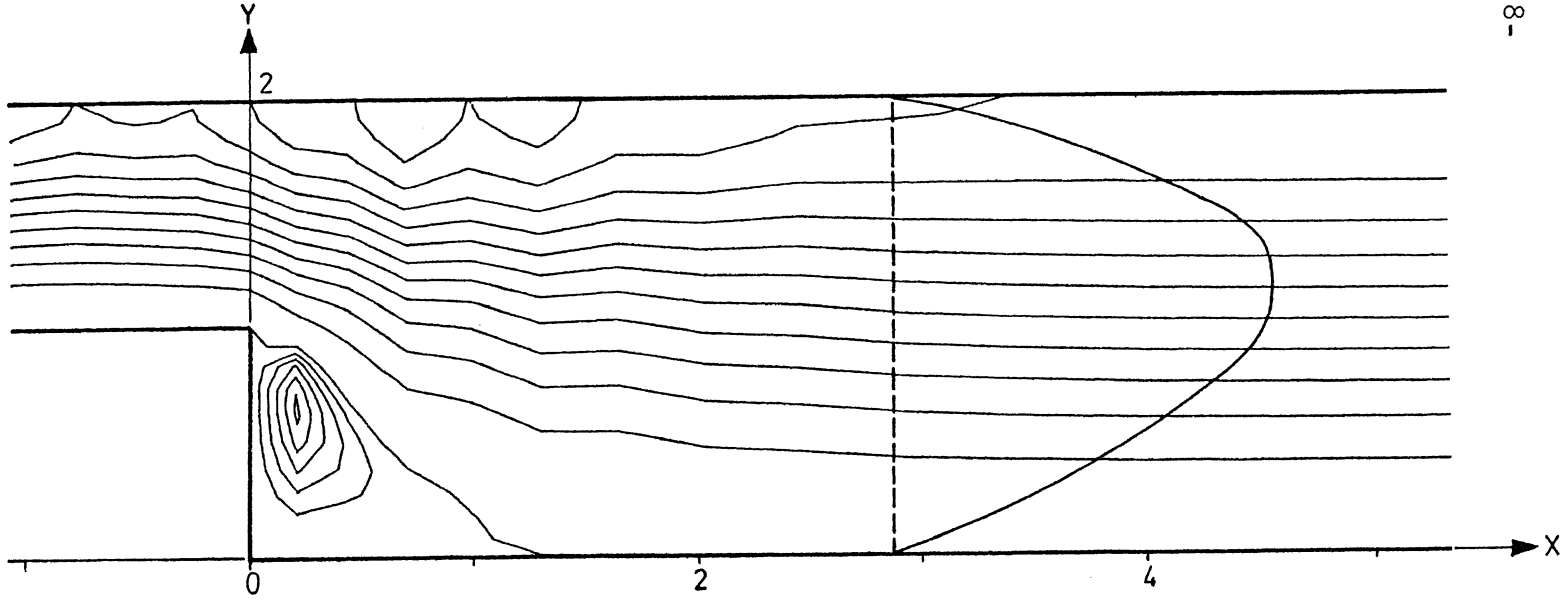

fig.3.4a: Initial streamline distribution and streamline distribution after 1 minute CPU TIME; channel with small inlet, Re=50

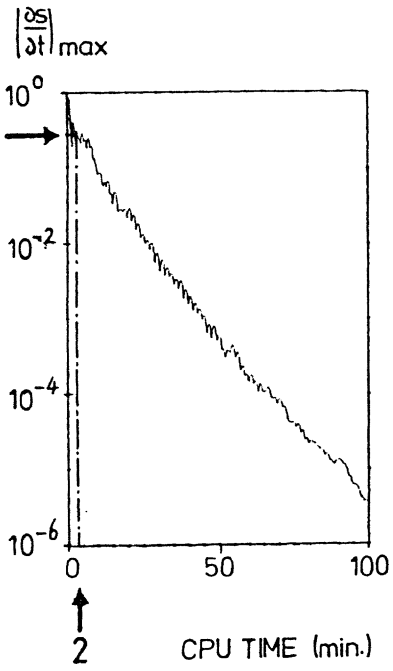

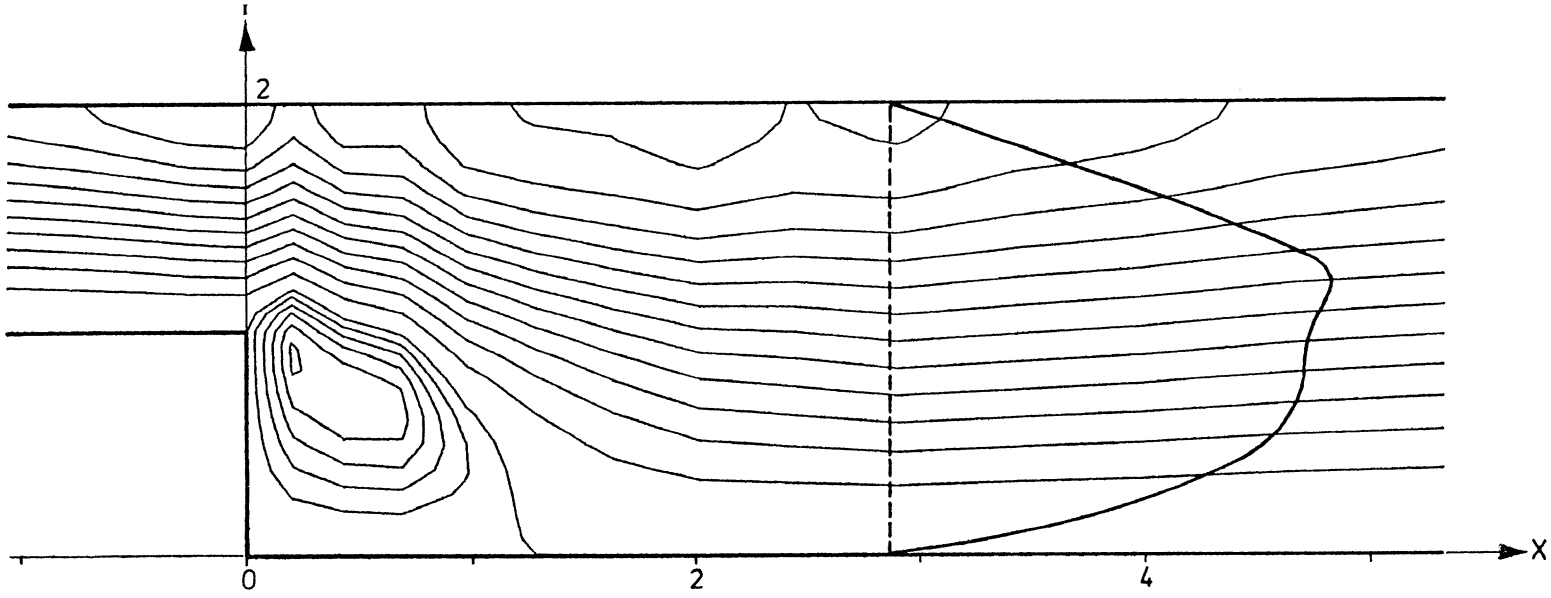

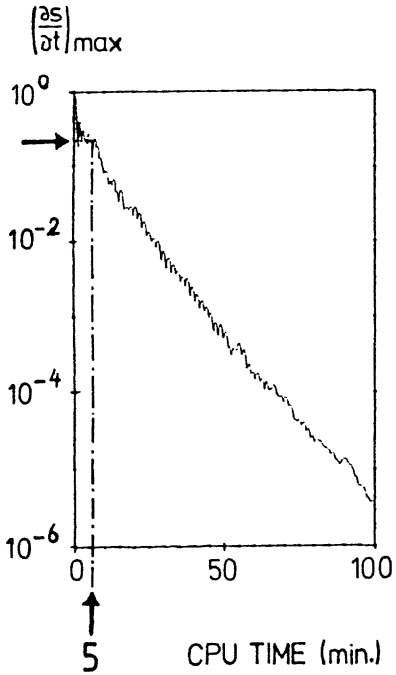

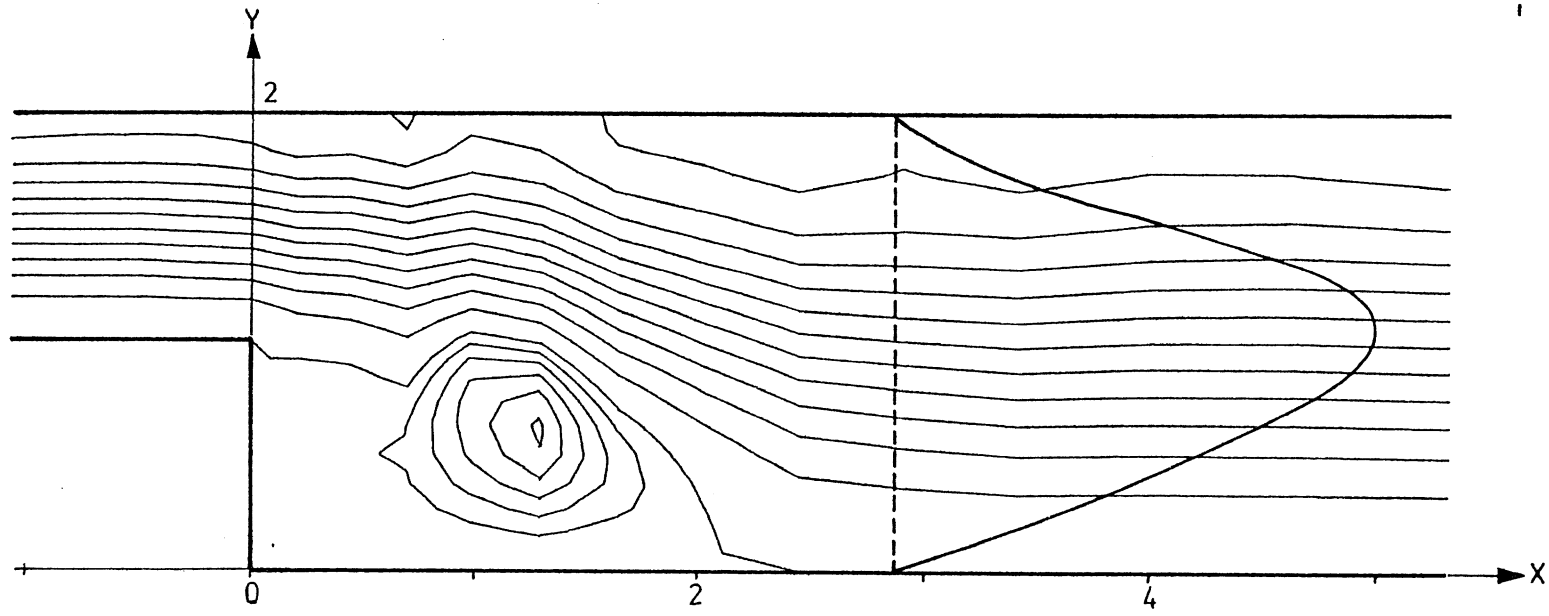

fig.3.4b: Streamline distribution after 2 and 5 minutes CPU TIME; channel with small inlet, Re=50

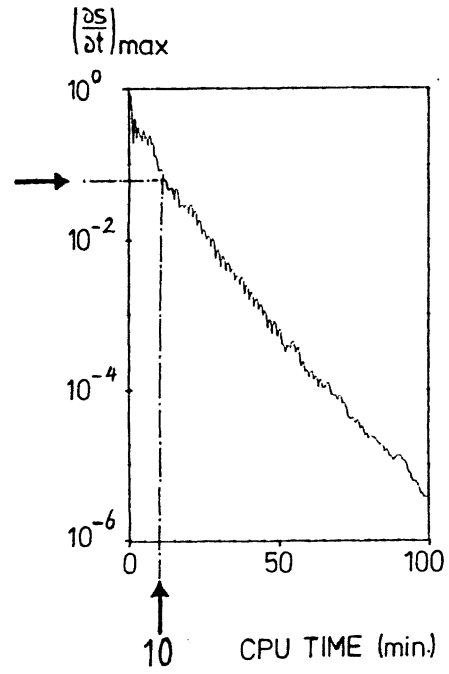

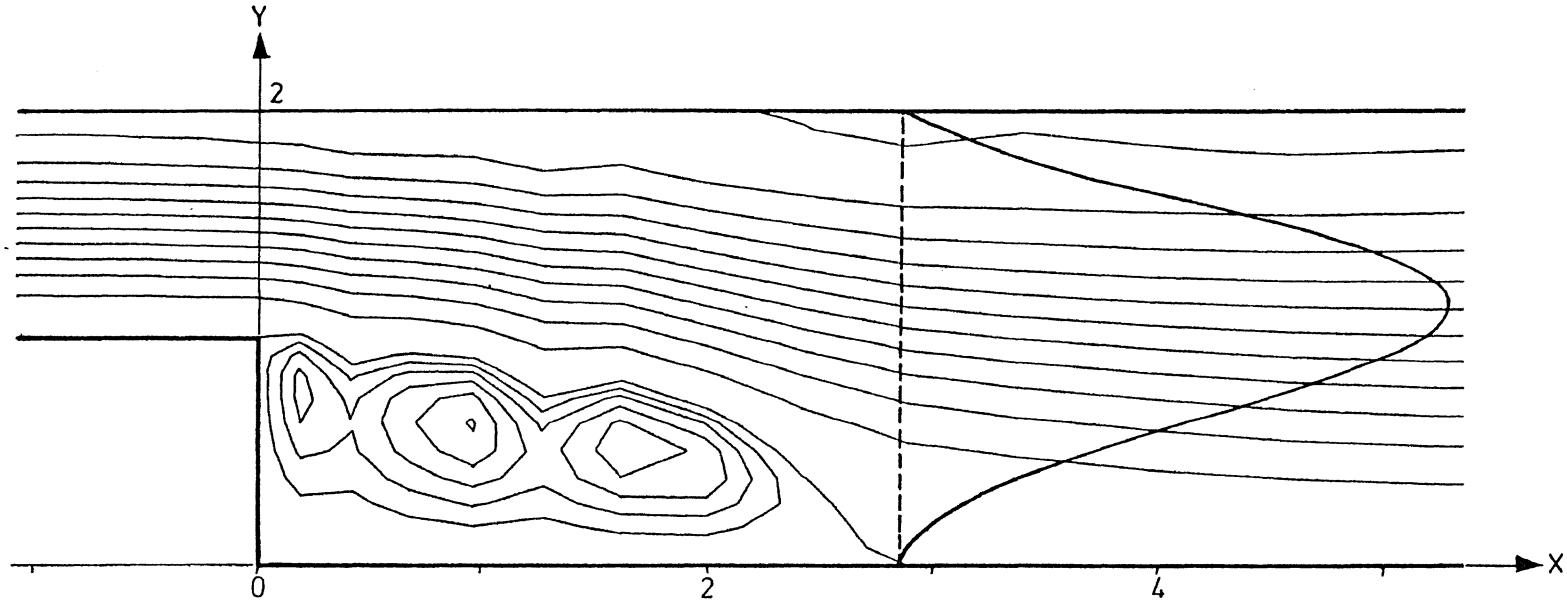

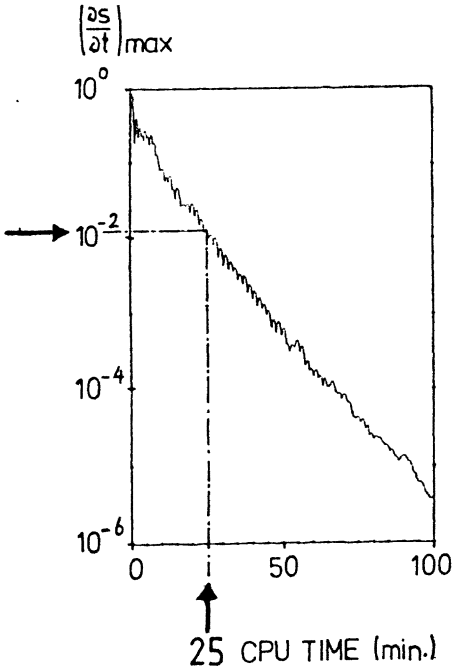

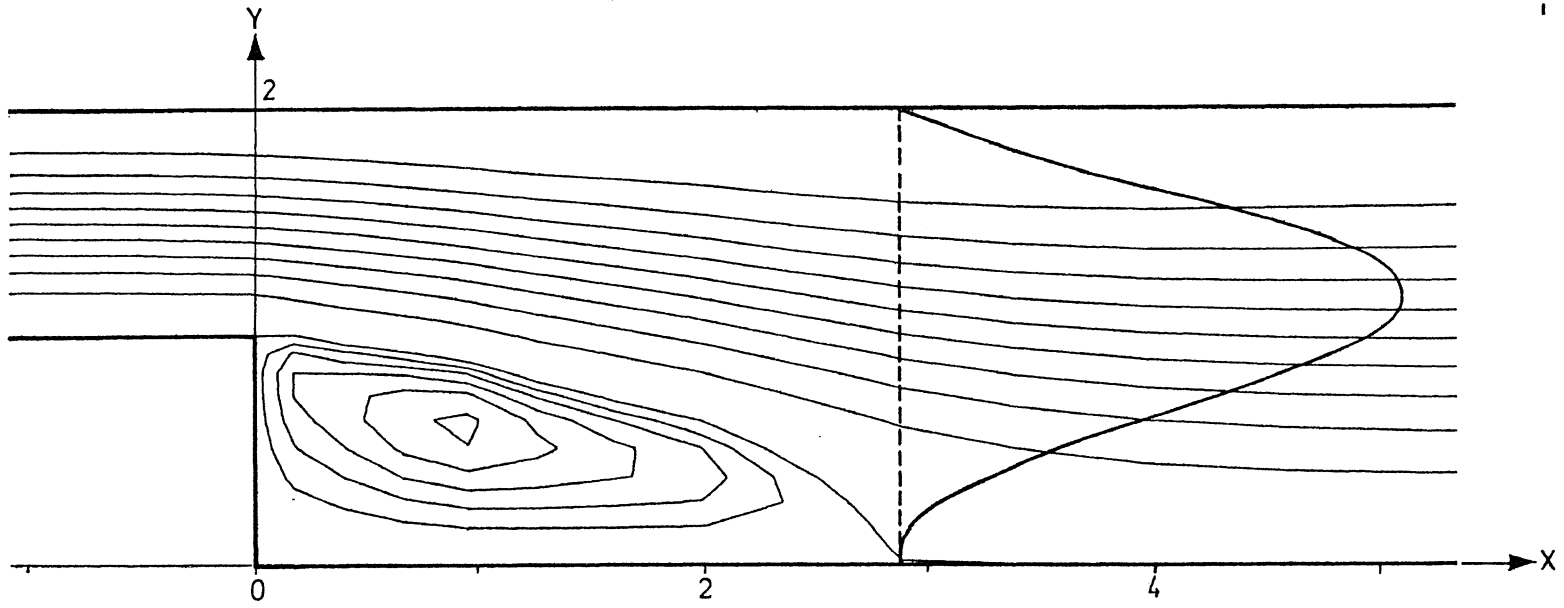

fig.3.4c: Streamline distribution after 10 and 25 minutes CPU TIME; channel with small inlet, Re=50

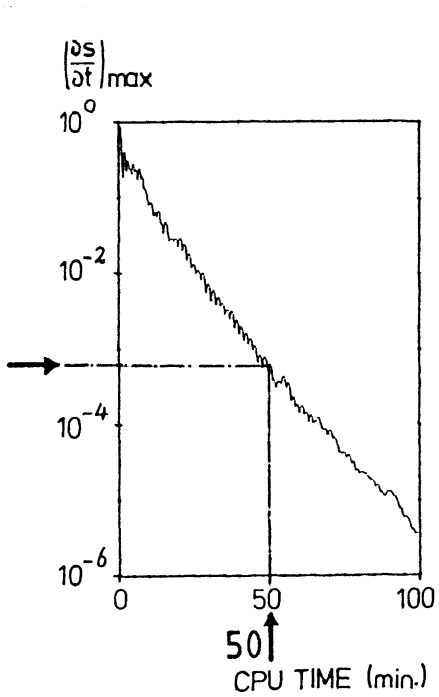

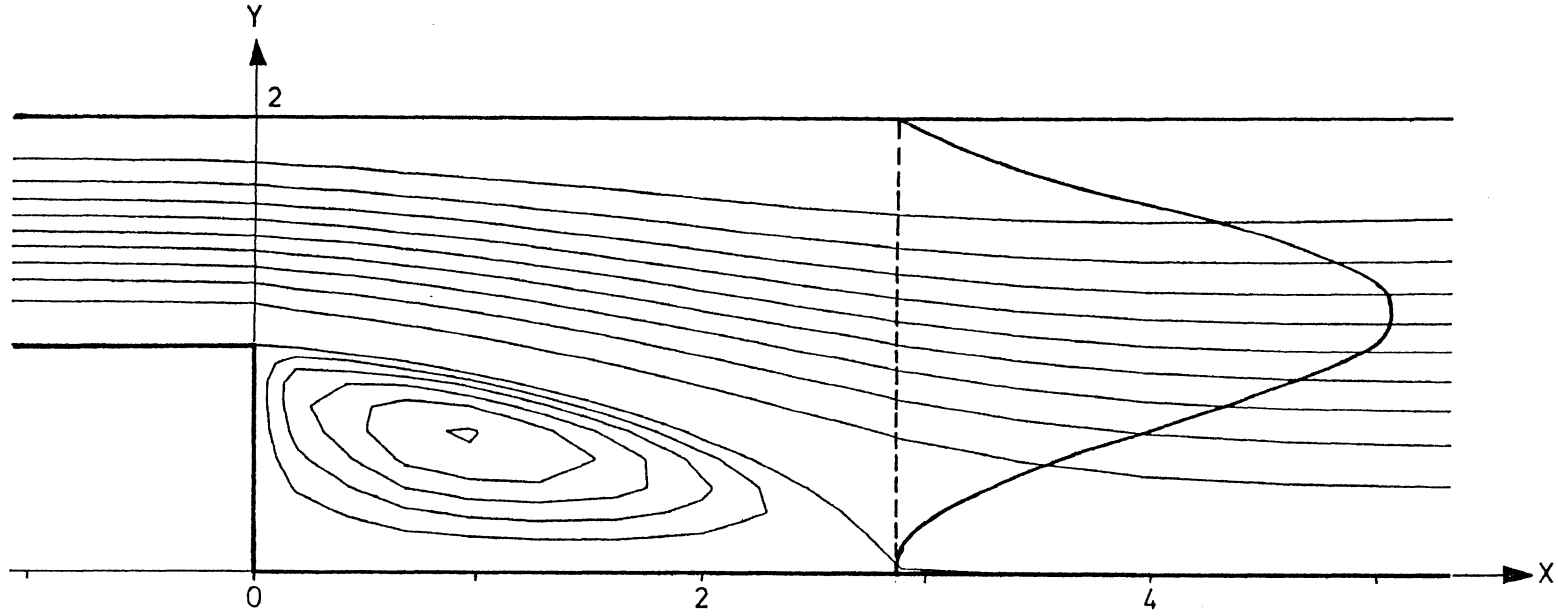

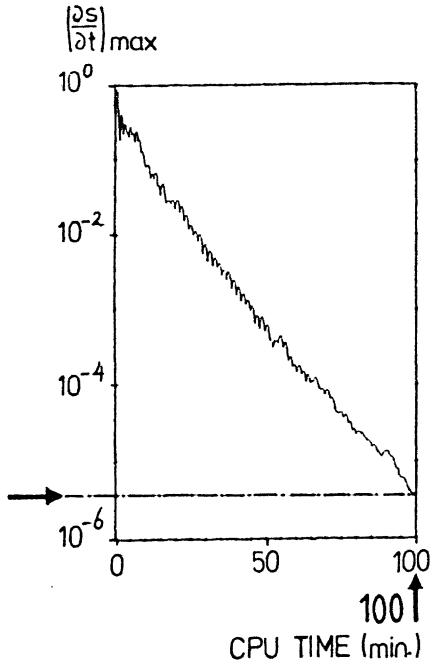

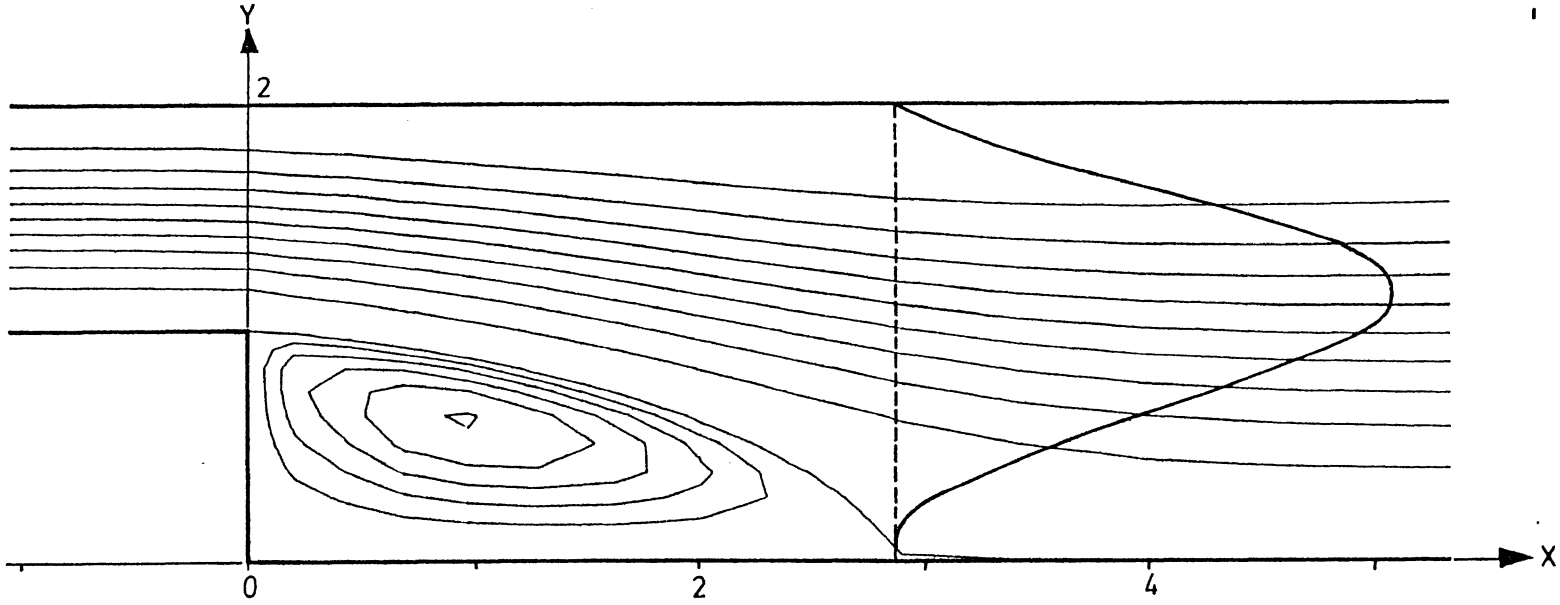

fig.3.4d: Streamline distribution after 50 and 100 minutes CPU TIME; channel with small inlet, Re=50

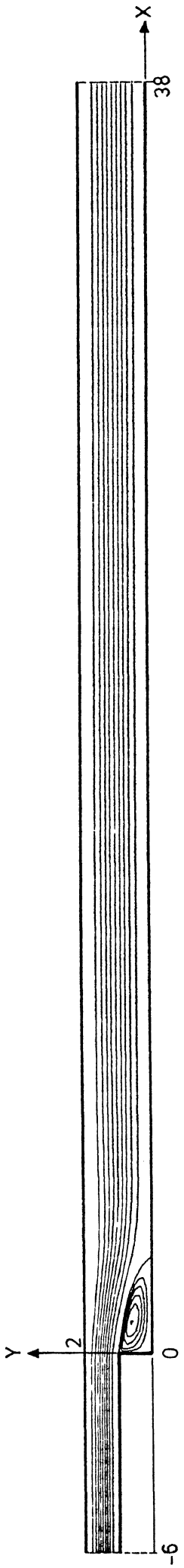

fig.3.5a: Streamline distribution; channel with small inlet, Re=50

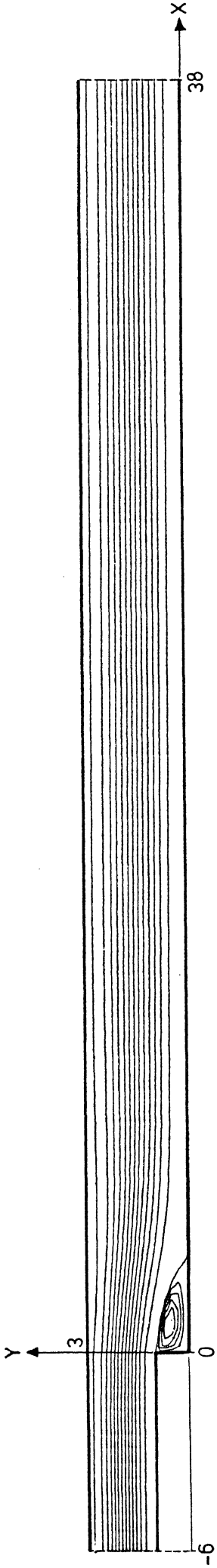

fig.3.5b: Streamline distribution; channel with big inlet, Re=50

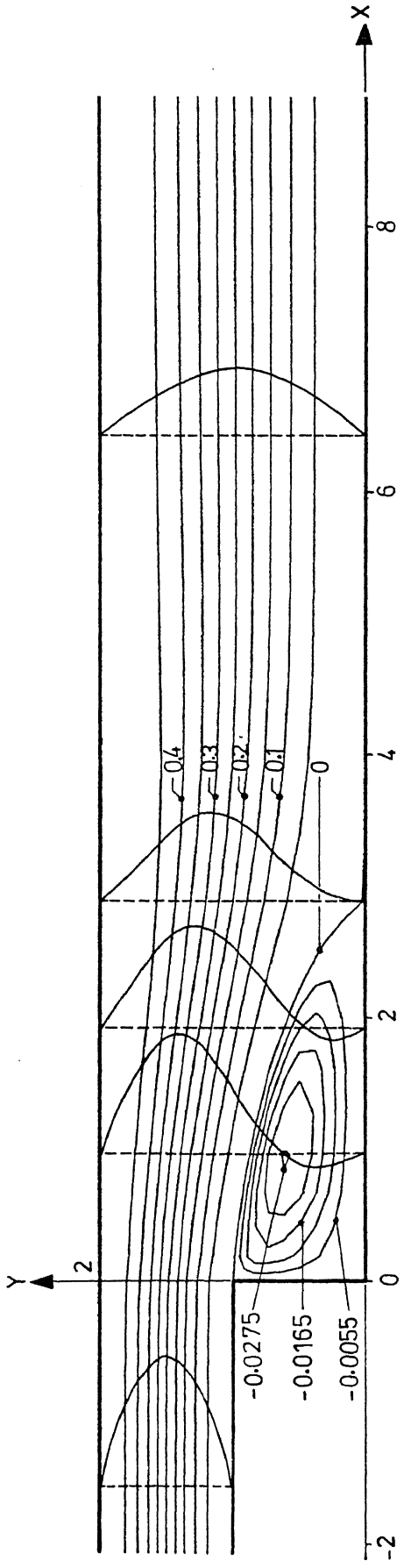

fig.3.6a: Streamline distribution; channel with small inlet, Re=50 (present results)

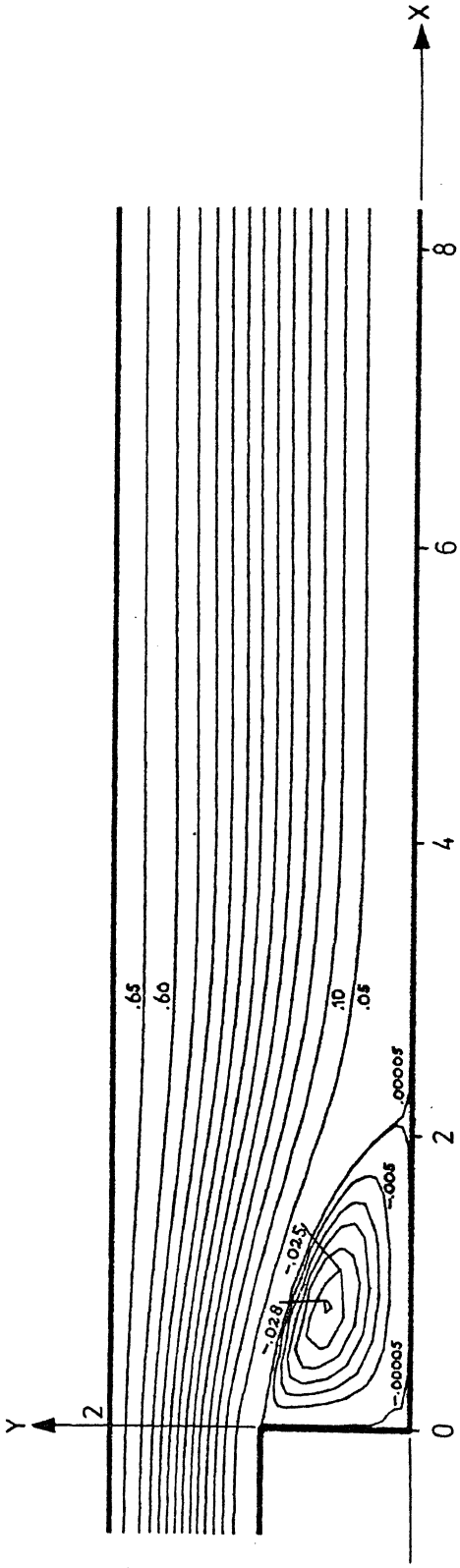

fig.3.6b: Streamline distribution; channel with small inlet, Re=50 (results Borsboom)

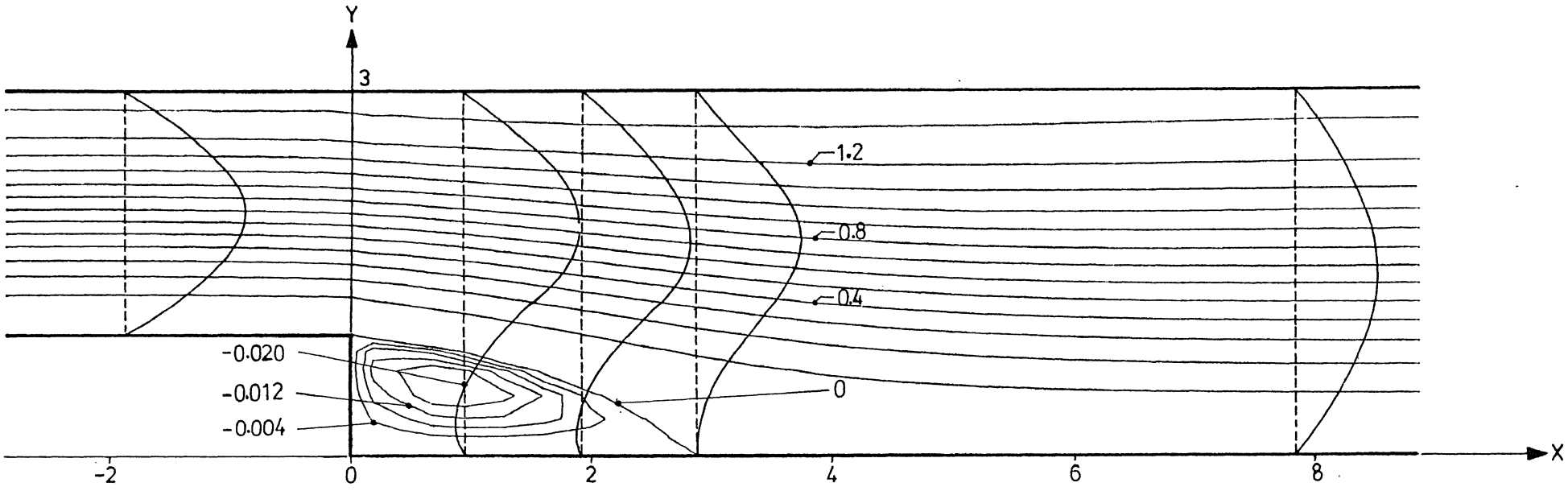

fig.3.7a: Streamline distribution; channel with big inlet, Re=50 (present results)

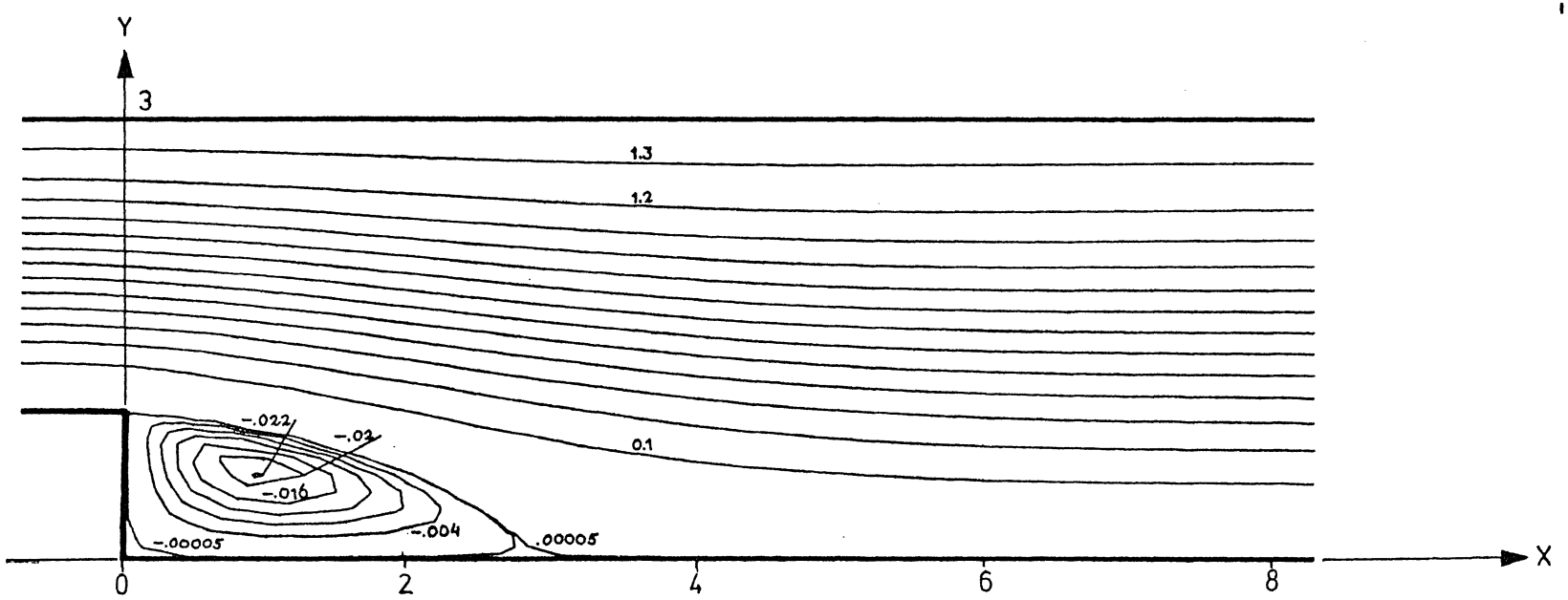

fig.3.7b: Streamline distribution; channel with big inlet, Re=50 (results Borsboom)

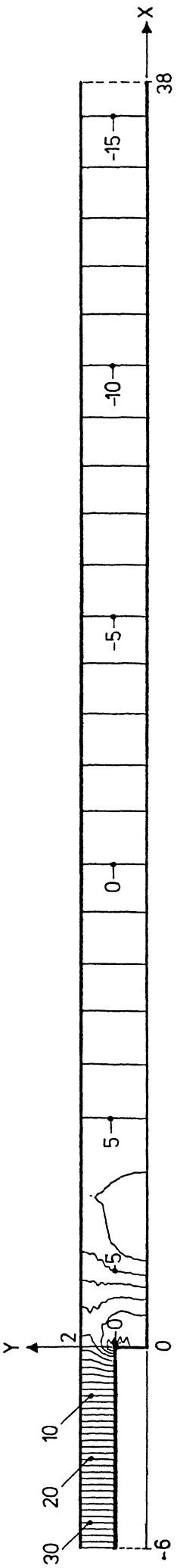

fig.3.8a: Pressure distribution; channel with small inlet, Re=50

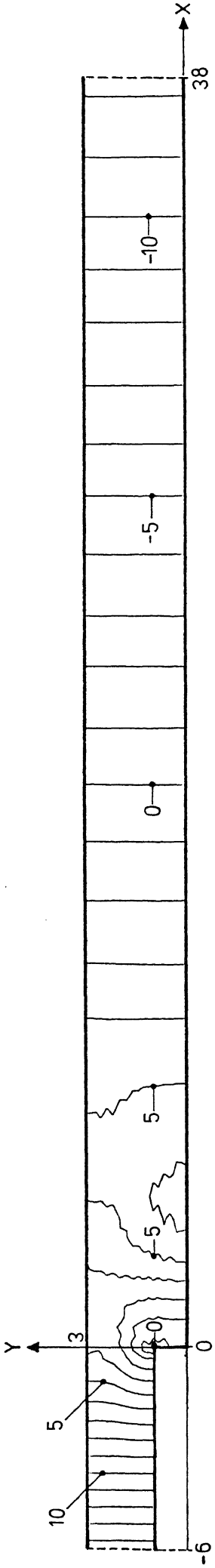

fig.3.8b: Pressure distribution; channel with big inlet, Re=50

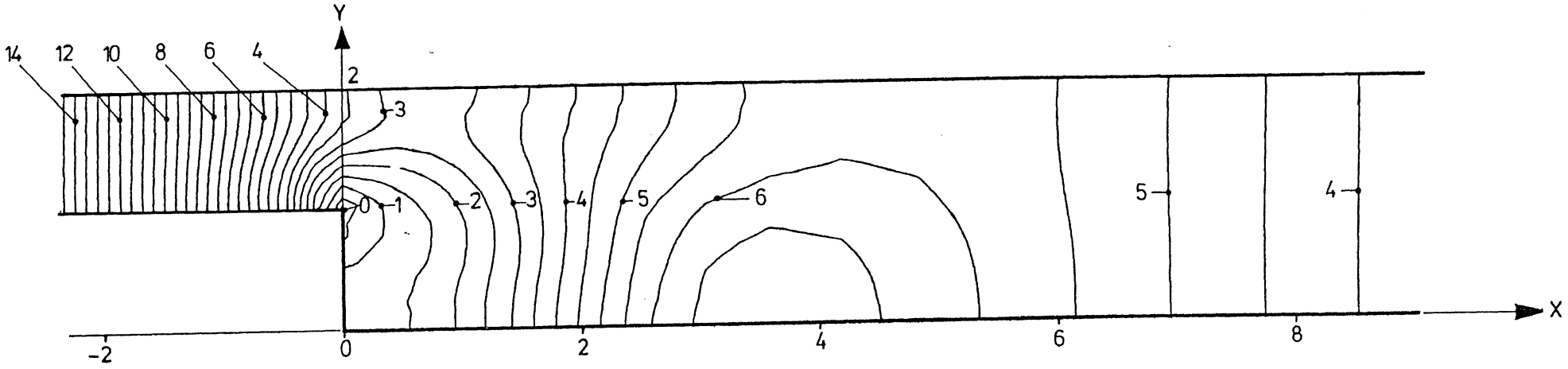

fig.3.9a: Smoothed pressure distribution; channel with small inlet, Re=50 (present results)

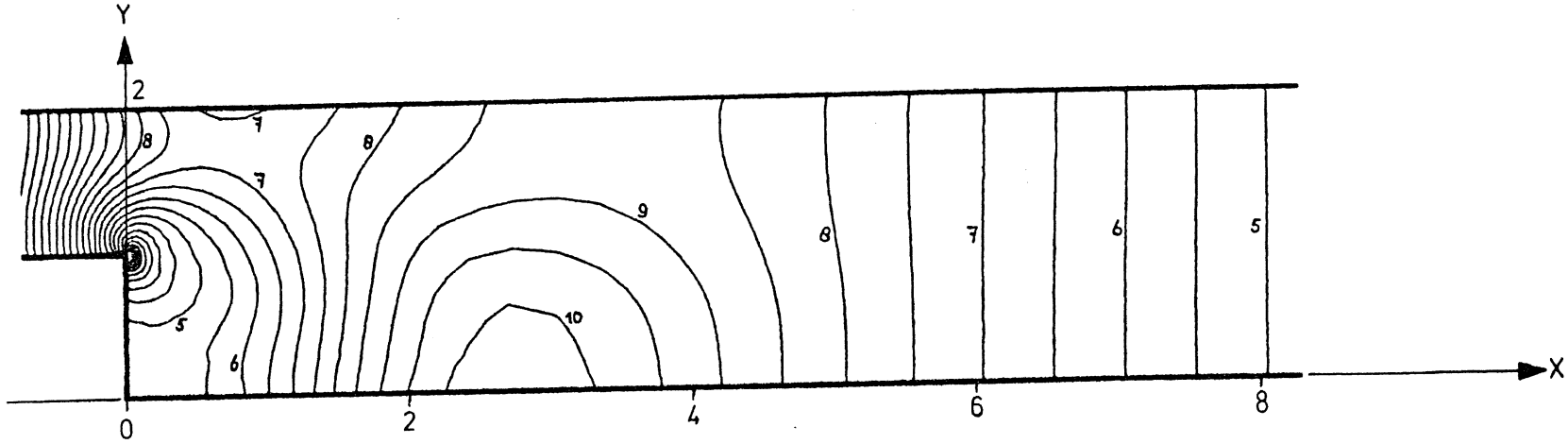

fig.3.9b: Non-smoothed pressure distribution; channel with small inlet, Re=50 (results Borsboom)

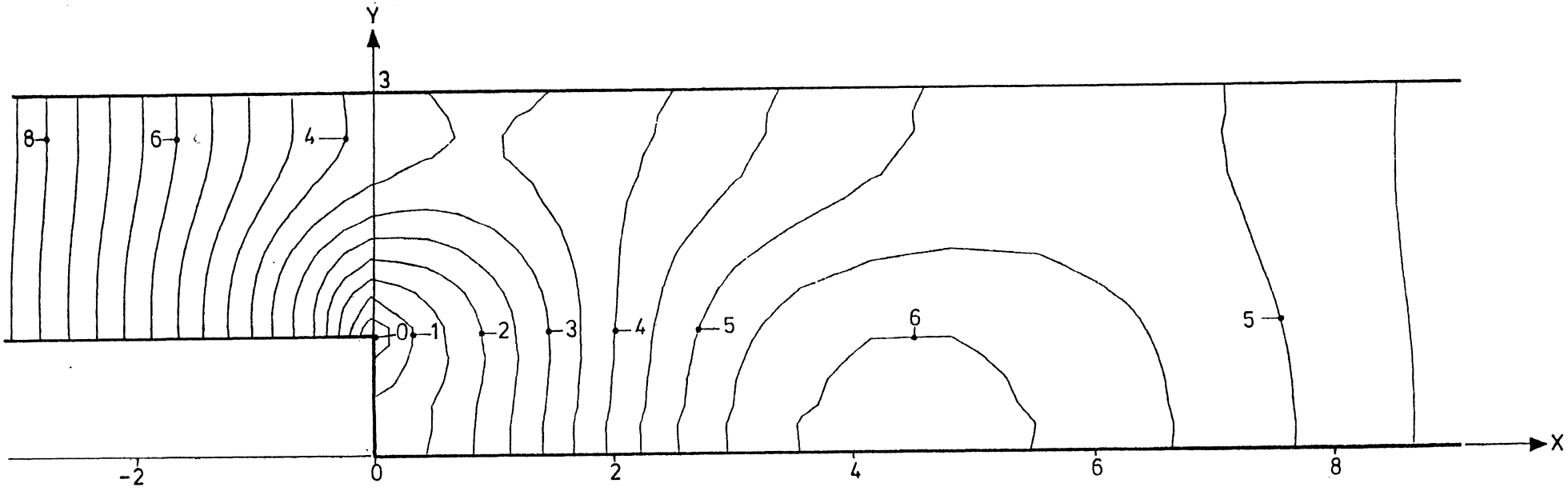

fig.3.10a: Smoothed pressure distribution; channel with big inlet, Re=50 (present results)

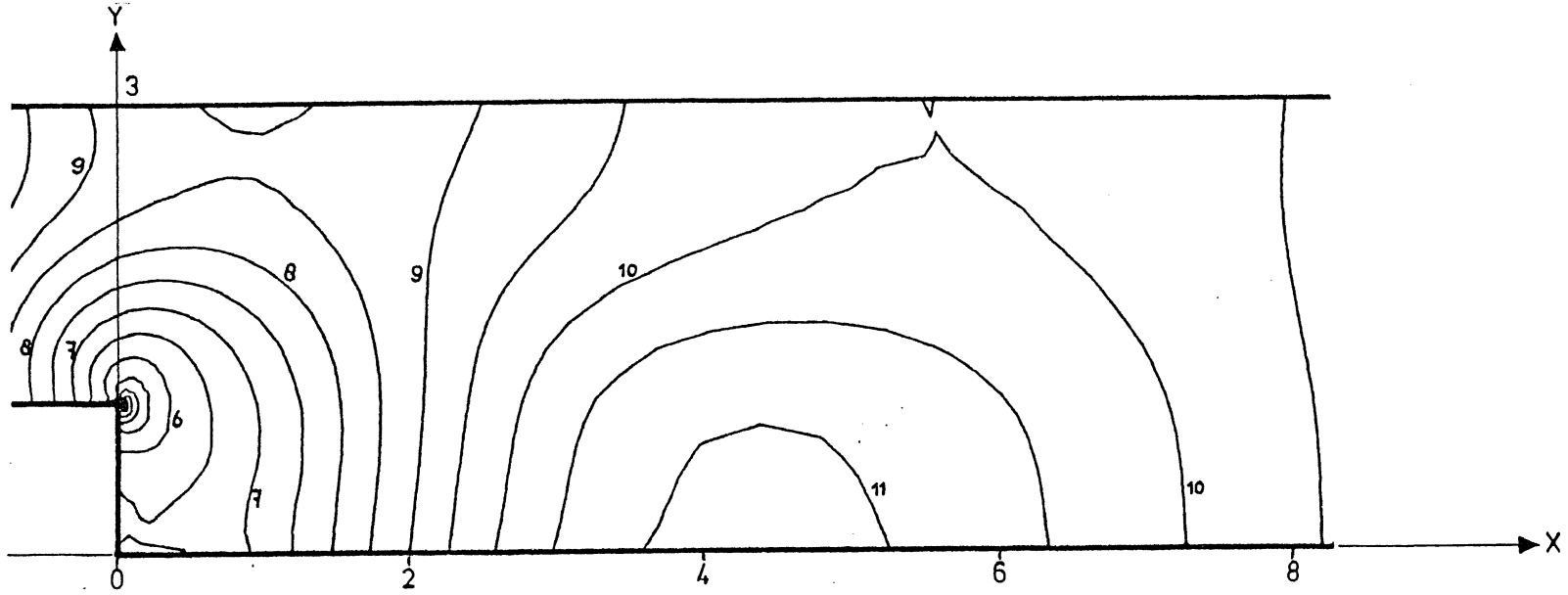

fig.3.10b: Non-smoothed pressure distribution; channel with big inlet, Re=50 (results Borsboom)

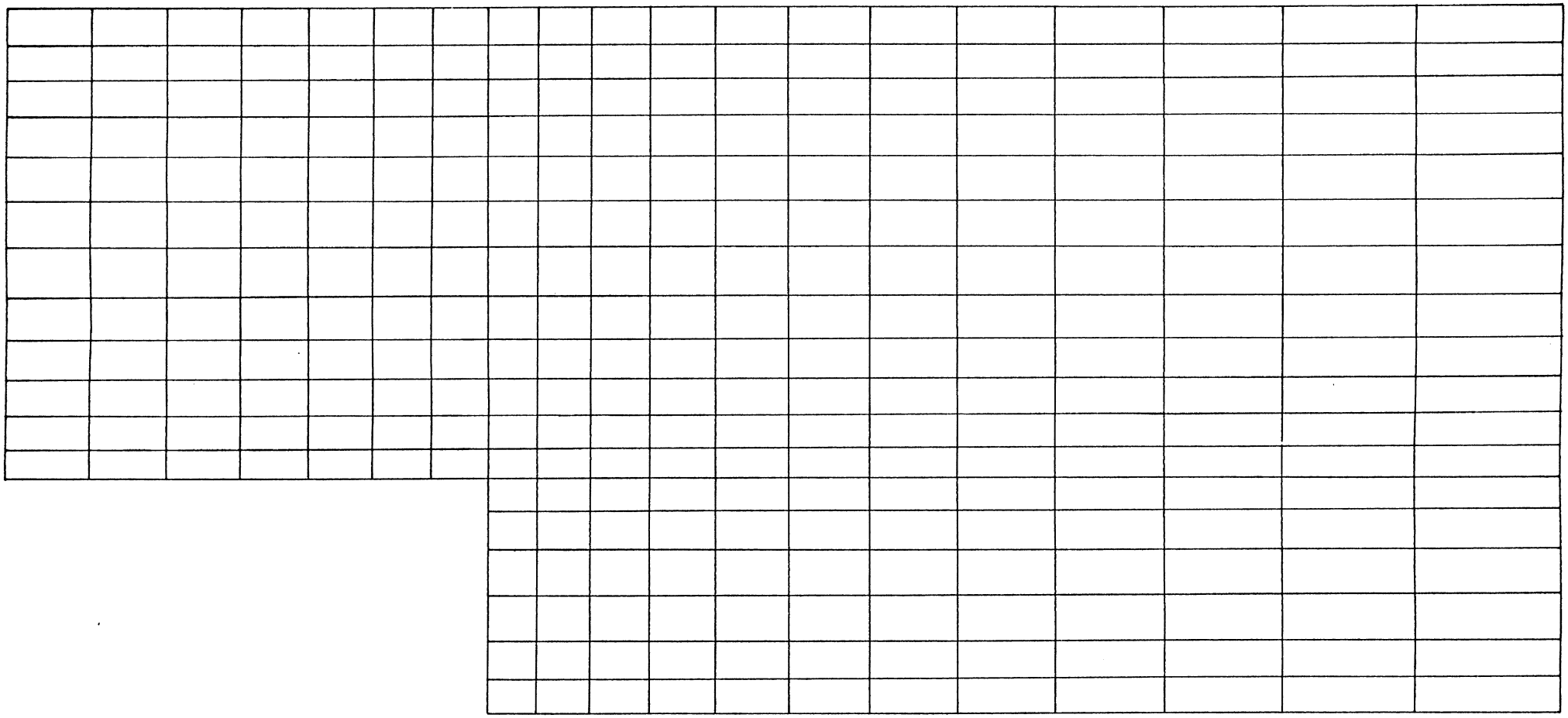

fig.3.11a: Present mesh; channel with big inlet

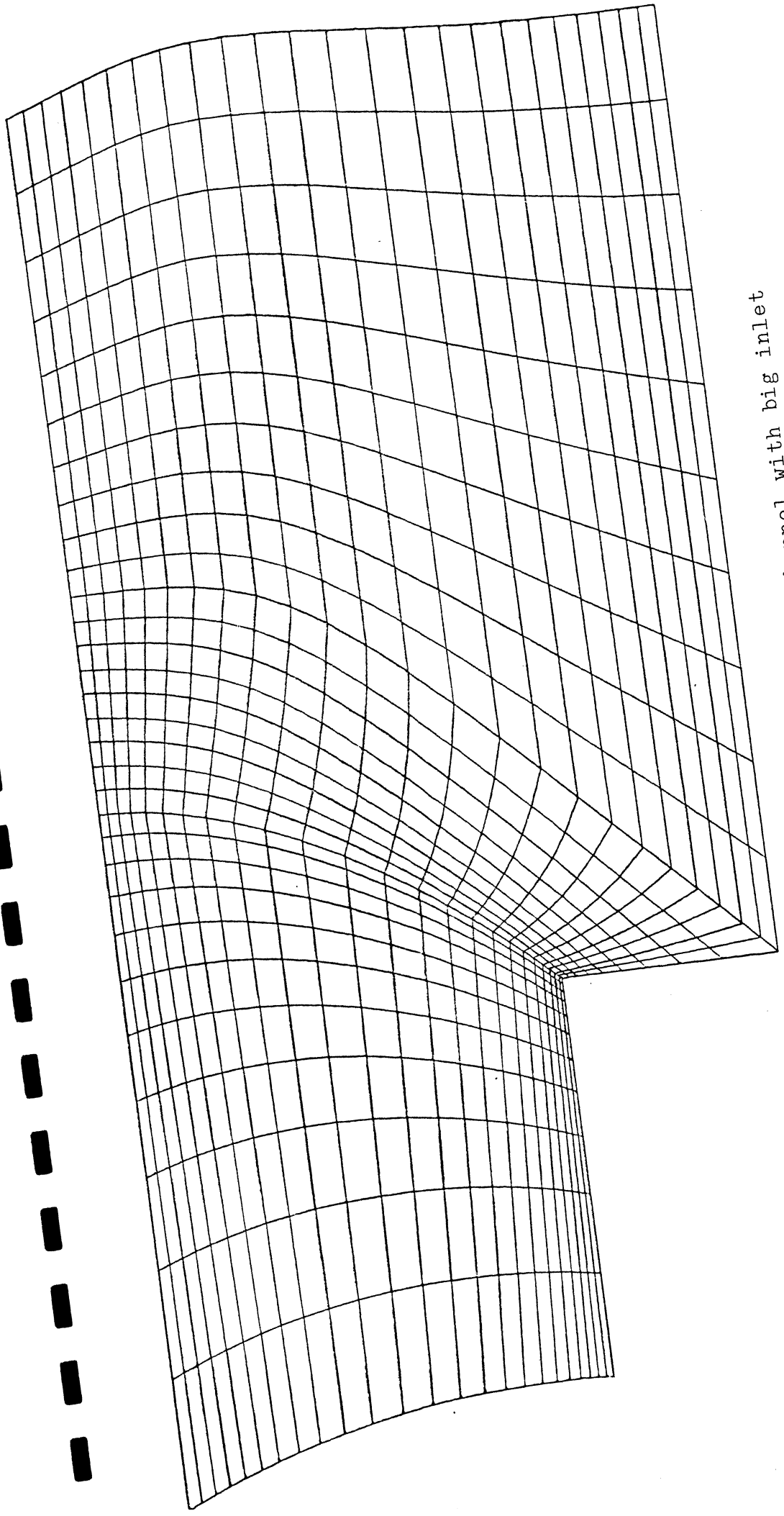

fig.3.11b: Mesh Borsboom; channel with big inlet

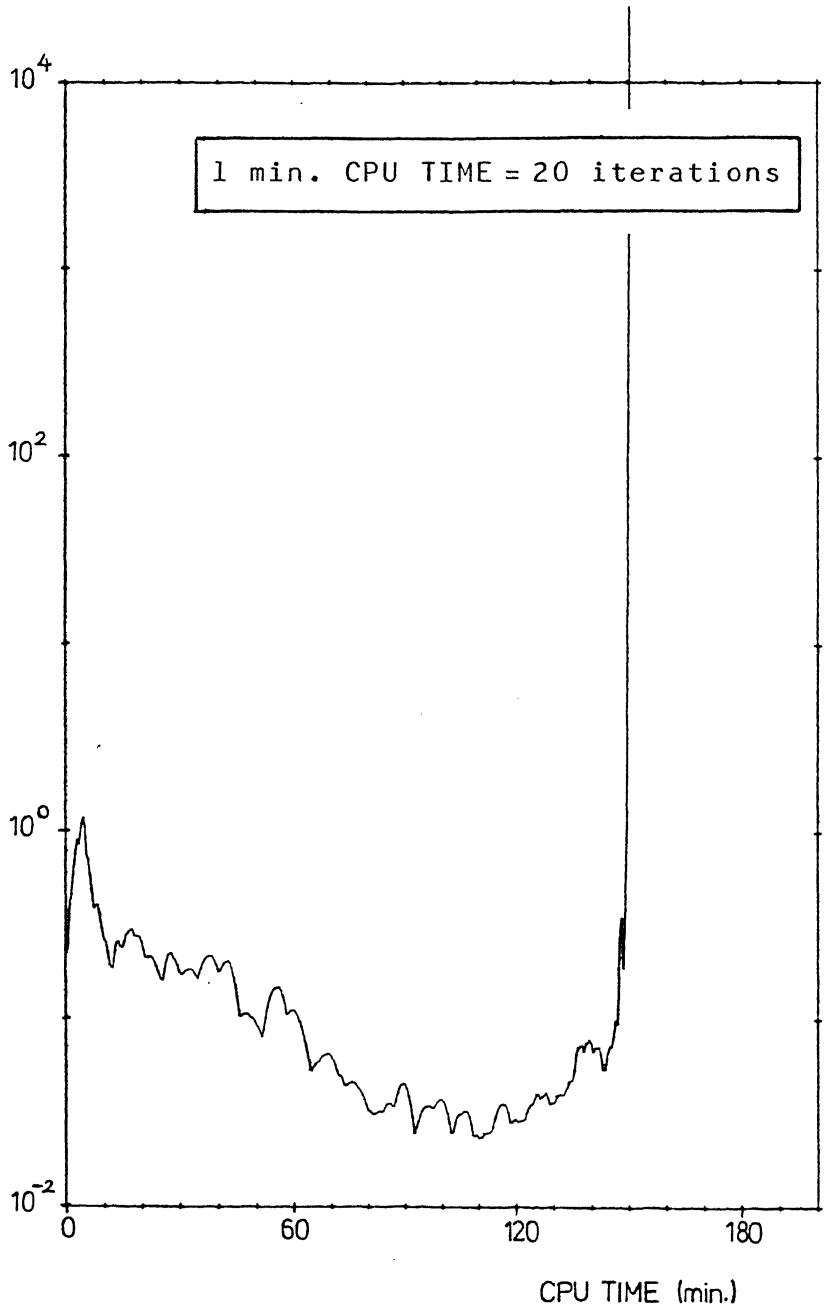

fig.3.12a: Divergence history; channel with small inlet, Re=150

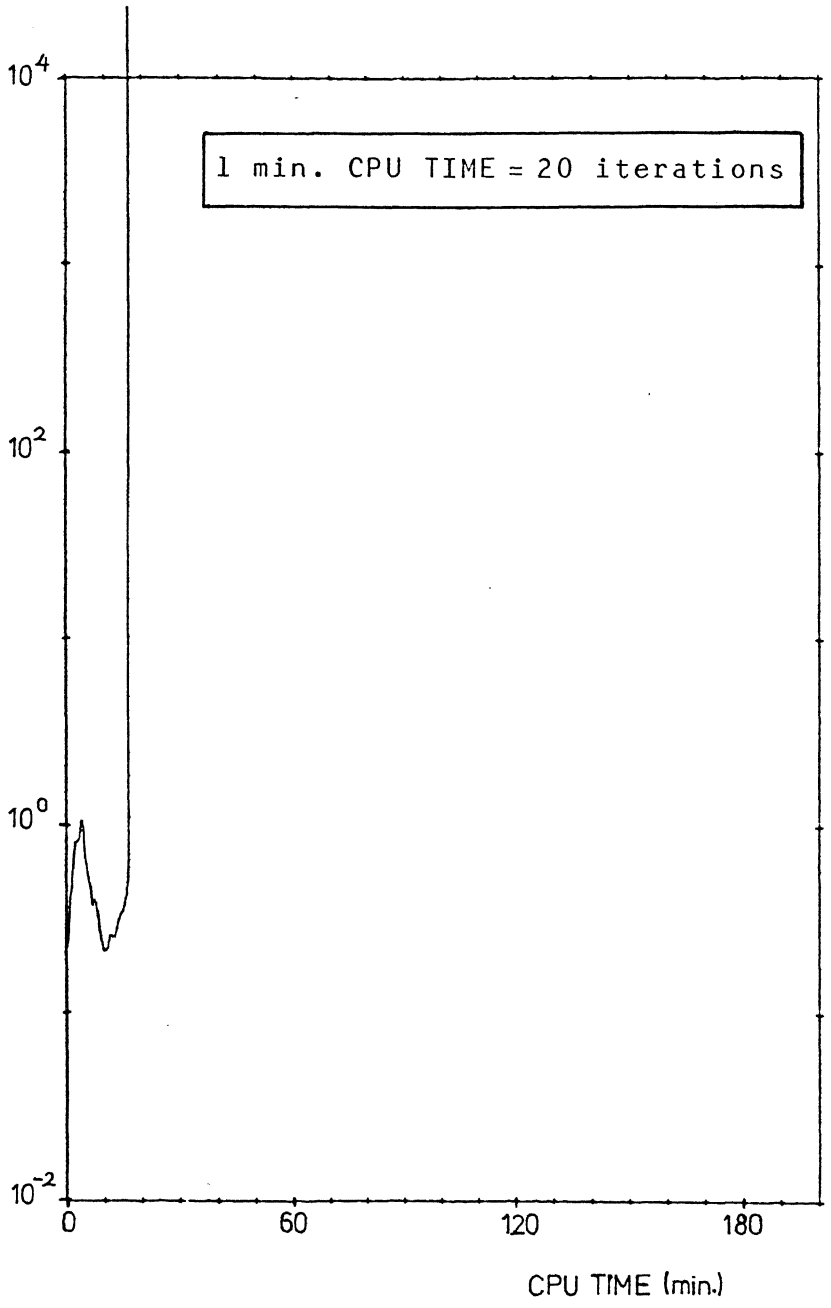

fig.3.12b: Divergence history; channel with small inlet, Re=500

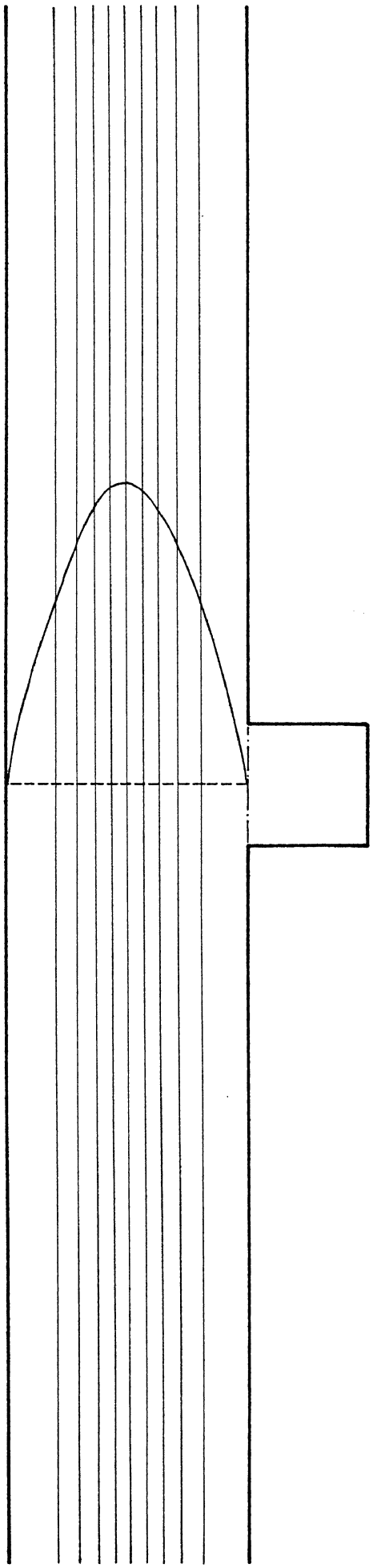

fig.3.13a: Initial streamline distribution channel with cavity, Re=50

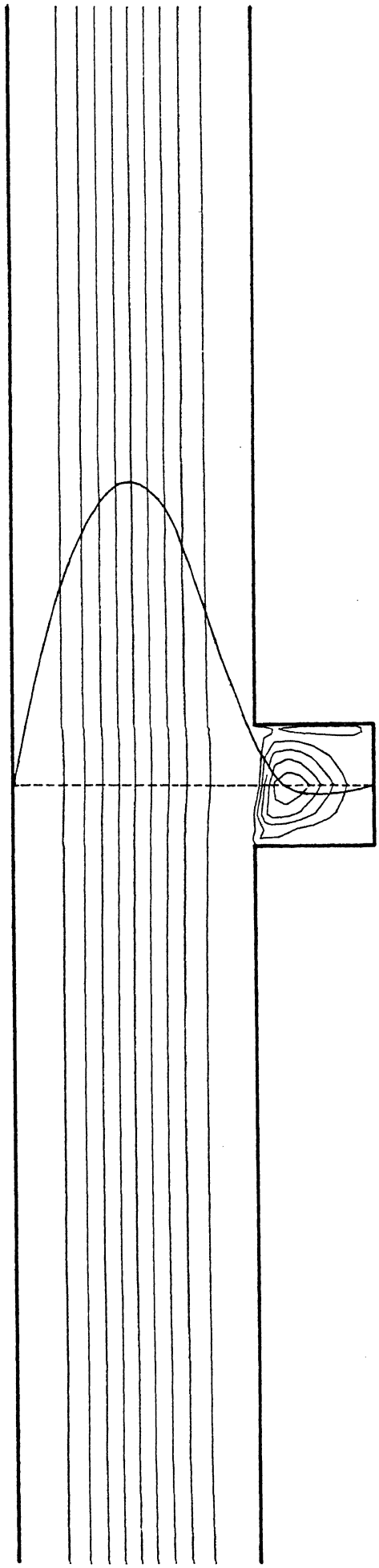

fig.3.13b: Converged streamline distribution channel with cavity, Re=50

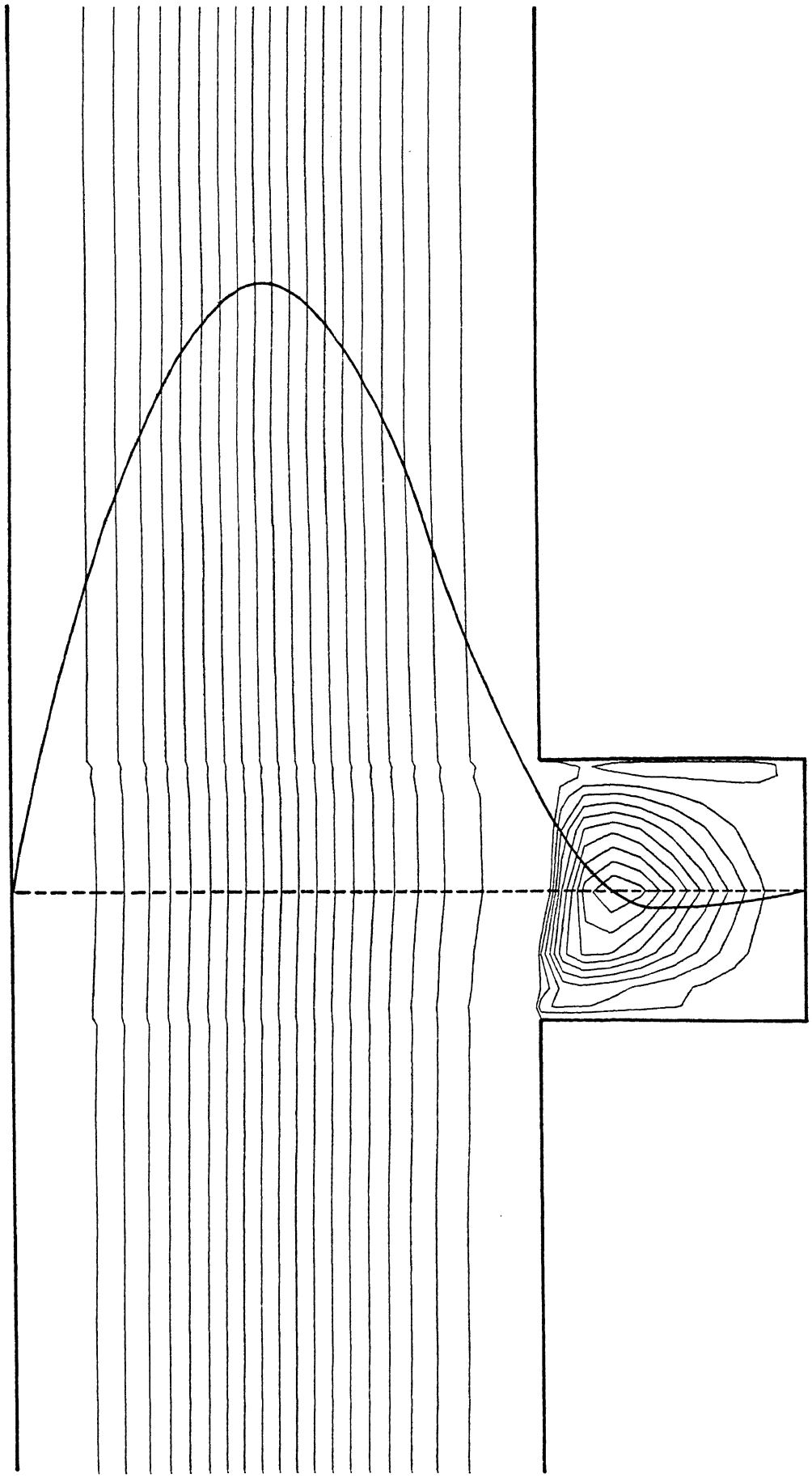

fig.3.13c: Detail converged streamline distribution channel with cavity, Re=50